Resonantly enhanced and diminished strong-field gravitational-wave fluxes

Éanna E. Flanagan,[1] Scott A. Hughes,[2–4] and Uchupol Ruangsri[2]

[1]*Center for Radiophysics and Space Research, Cornell University, Ithaca, New York 14853, USA*
[2]*Department of Physics and MIT Kavli Institute, MIT, Cambridge, Massachusetts 02139, USA*
[3]*Canadian Institute for Theoretical Astrophysics, University of Toronto, 60 St. George Street, Toronto, Ontario M5S 3H8, Canada*
[4]*Perimeter Institute for Theoretical Physics, Waterloo, Ontario N2L 2Y5, Canada*

(Received 19 August 2012; published 7 April 2014)

The inspiral of a stellar mass ($1 - 100M_\odot$) compact body into a massive ($10^5 - 10^7 M_\odot$) black hole has been a focus of much effort, both for the promise of such systems as astrophysical sources of gravitational waves, and because they are a clean limit of the general relativistic two-body problem. Our understanding of this problem has advanced significantly in recent years, with much progress in modeling the "self-force" arising from the small body's interaction with its own spacetime deformation. Recent work has shown that this self-interaction is especially interesting when the frequencies associated with the orbit's θ and r motions are in an integer ratio: $\Omega_\theta/\Omega_r = \beta_\theta/\beta_r$, with β_θ and β_r both integers. In this paper, we show that key aspects of the self-interaction for such "resonant" orbits can be understood with a relatively simple Teukolsky-equation-based calculation of gravitational-wave fluxes. We show that fluxes from resonant orbits depend on the relative phase of radial and angular motions. The purpose of this paper is to illustrate in simple terms how this phase dependence arises using tools that are good for strong-field orbits, and to present a first study of how strongly the fluxes vary as a function of this phase and other orbital parameters. Future work will use the full dissipative self-force to examine resonant and near resonant strong-field effects in greater depth, which will be needed to characterize how a binary evolves through orbital resonances.

DOI: 10.1103/PhysRevD.89.084028 PACS numbers: 04.30.-w, 04.25.Nx, 04.70.-s

I. INTRODUCTION

A. The self-force driven evolution of binaries: A very brief synopsis

Our understanding of the two-body problem in general relativity has advanced substantially in the past decade. Besides the celebrated breakthroughs in numerical relativity [1–3] which have opened the field of binary phenomenology in general relativity, there has been great progress in understanding the extreme mass-ratio limit of this problem, when one member of the binary is much smaller than the other. This limit is of great interest in describing astrophysical extreme mass-ratio binaries (a particularly interesting source for space-based gravitational-wave measurements) [4], and as a limiting form of the more generic two-body problem [5,6].

Most efforts to model extreme mass-ratio binaries have focused on the computation of *self-forces* (see Ref. [7] for a recent comprehensive review). Consider a small body orbiting a black hole. At zeroth order in the small body's mass, its motion is described as a geodesic of the black hole spacetime. At first order in this mass, the black hole's spacetime is slightly deformed. This deformation changes the trajectory that the small body follows, pushing it away from the background spacetime's geodesic. It is useful to regard the change to the trajectory as arising from a self-force which modifies the geodesic equations typically used to describe black hole orbits. Conceptually, it is useful to split the self-force into two pieces: a time-symmetric *conservative* piece and a time-asymmetric *dissipative* piece. On average, the impact of the conservative contribution is to shift orbital frequencies away from their geodesic values. The dissipative self-force is equivalent, on average, to a slow evolution of the otherwise conserved constants (e.g., the orbital energy and angular momentum) which characterize geodesic orbits. It makes the largest contribution to an orbit's phase evolution. The conservative piece makes a smaller (though still significant) contribution which accumulates secularly over many orbits [8,9].

Recent work by Flanagan and Hinderer [10] (hereafter FH) using a post-Newtonian (pN) approximation to the self-force together with fully relativistic orbital dynamics has shown that a small body's self-interaction becomes particularly important near *resonances*. The background geodesic motion can be characterized by three orbital frequencies with respect to Boyer-Lindquist time: a radial frequency Ω_r, a polar frequency Ω_θ, and an axial frequency Ω_ϕ. In the weak-field (large separation) limit, these three frequencies asymptote to the Newtonian Kepler frequency. In the strong field, these frequencies can differ significantly, with Ω_r always the smallest frequency (the relative magnitude of Ω_θ and $|\Omega_\phi|$ depends on the sign of the orbit's axial angular momentum). Resonant orbits are ones for which the radial and angular motions become

commensurate: $\Omega_\theta/\Omega_r = \beta_\theta/\beta_r$, where β_θ and β_r are small integers with no common factors. On such orbits, components of the self-interaction which normally "average away" when examined over a full orbital period instead combine coherently, substantially changing their impact on the system's evolution.

For the purpose of our background discussion, it is useful to include more details from FH's analysis of how resonant effects arise. Consider a body of mass μ moving on a bound trajectory near a Kerr black hole of mass M, with $\mu \ll M$. FH note that one can describe the motion of this body using action-angle variables and correctly accounting for how the integrals which parametrize geodesic orbits evolve due to the self-force. Writing the angle variables $q_\alpha = (q_t, q_r, q_\theta, q_\phi)$ (which describe motions in the t, r, θ, and ϕ directions of Boyer-Lindquist coordinates), and writing the integrals associated with geodesic motion $J_i = (E, L_z, Q)$ (with E the energy, L_z the axial angular momentum, and Q the Carter constant), the equations of motion describing the system are [12]

$$\frac{dq_\alpha}{d\tau} = \omega_\alpha(\mathbf{J}) + \epsilon g_\alpha^{(1)}(q_r, q_\theta, \mathbf{J}) + O(\epsilon^2), \tag{1.1}$$

$$\frac{dJ_i}{d\tau} = \epsilon G_i^{(1)}(q_r, q_\theta, \mathbf{J}) + O(\epsilon^2). \tag{1.2}$$

The time parameter τ is proper time along the orbit; the parameter $\epsilon = \mu/M$ is the system's mass ratio. The $\omega_{r,\theta,\phi}$ are fundamental frequencies with respect to proper time associated with bound Kerr geodesic orbits. The forcing functions $g_\alpha^{(1)}$ and $G_i^{(1)}$ arise from the first-order self-force. FH also include discussion of second-order forcing functions, which we do not need for this synopsis; see Ref. [10] for further discussion.

At order ϵ^0, Eqs. (1.1) and (1.2) simply describe geodesics of Kerr black holes: The integrals of the motion are constant, and each angle variable evolves according to its associated frequency. The leading adiabatic dissipative correction to this motion can be found by dropping the forcing term $g_\alpha^{(1)}$ and replacing $G_i^{(1)}$ by $\langle G_i^{(1)} \rangle$, the average of this forcing term over the 2-torus parametrized by q_θ and q_r [12]. To compute this torus-averaged self-force, it is sufficient to use the radiative approximation [9,11,12], which includes only the radiative contributions to the self-interaction and neglects conservative contributions. For generic (nonresonant) orbits, this torus average coincides with an infinite time average, and the averaged quantities $\langle G_i^{(1)} \rangle$ are just the time-averaged fluxes of energy, angular momentum, and Carter constant. In recent years such time-averaged fluxes have been computed numerically using the frequency domain Teukolsky equation [23–25]. These fluxes can be used to compute leading-order, adiabatic inspirals. The conservative contributions influence the motion only beyond the leading adiabatic order [11,12].

B. Resonant effects

Now consider going beyond the leading adiabatic order. Important post-adiabatic effects can be found by continuing to neglect $g_\alpha^{(1)}$, but now integrating Eq. (1.2) using $G_i^{(1)}$ rather than its averaged variant. FH show that for "most" orbits, $G_i^{(1)}$ is given by $\langle G_i^{(1)} \rangle$ plus a rapidly oscillating contribution. Over the time scales associated with inspiral, this rapidly oscillating piece averages away and has little effect. The effect of the forcing term $G_i^{(1)}$ is dominated by $\langle G_i^{(1)} \rangle$ for all nonresonant orbits.

For resonant orbits, this averaging fails: contributions beyond $\langle G_i^{(1)} \rangle$ are *not* rapidly oscillating and can significantly modify how the integrals of motion evolve during an inspiral. A given binary is very likely to evolve through several low-order resonances en route to the final merger of the smaller body with the large black hole [13]. A complete quantitative understanding of these resonant effects will thus be quite important for making accurate inspiral models. Prior to FH's analysis, several other papers argued that such resonances may play an important role in the radiative evolution of binary systems [14,15] (albeit without quantifying the detailed impact they can have), or else because of other effects which resonances have on the evolution of a dynamical system [16].

Orbits in which Ω_θ/Ω_r take on a small-integer ratio have been studied in great detail by Grossman, Levin, and Perez-Giz [17], who called them "periodic" orbits and provided a fairly simple scheme for classifying their features. Following Ref. [10] (as well as more recent work by Grossman, Levin, and Perez-Giz [18]), we will call them "resonant" orbits, reflecting the fact that our main interest is in understanding how their periodic structure impacts the self-interaction. Grossman, Levin, and Perez-Giz have more recently argued for the utility of using resonant orbits as sample points in numerical computations of leading order, adiabatic inspirals: evaluating fluxes at resonant orbits may enable a speedup of flux computations [18], more efficiently covering the parameter space of generic orbits. Although their goals are rather different from ours here, many of their techniques and results substantially overlap with ours (modulo minor differences in notation). We highlight the overlap at appropriate points in this paper.

As a binary evolves through a resonance, its self-interaction and thus its evolution are modified compared to what we would expect if the resonance were not taken into account. The details of how the self-interaction is modified depend on the relative phase of the radial and angular motions as the orbit passes through resonance. Because of this, *resonances enhance the dependence of a binary's orbital evolution on initial conditions.* Let the phase variable χ_0 define the value of the orbit's θ angle at the moment it reaches periapsis (see Sec. II A for more details). On resonance, two orbits which have the same energy E, the same axial angular momentum L_z, and the

same Carter constant Q will evolve differently if they have different values of χ_0.

FH estimate [10] that the shift to the orbital phase induced by these resonances can be several tens to $\sim 10^2$ rad for mass ratios $\sim 10^{-6}$ (as compared to an analysis which neglects the resonances). That there is such a large shift, and that this shift may depend on initial conditions, is potentially worrisome. Resonances could significantly complicate our ability to construct models for measuring the waves from extreme mass-ratio inspirals. On the other hand, the detailed behavior of a system as it evolves through resonances may offer an opportunity to study an interesting aspect of strong-field gravity, providing a new handle for strong-gravity phenomenology. Analytic studies of the effect of the passage through resonance can be found in Refs. [19,20].

C. Our analysis

The "several tens to $\sim 10^2$ rad" estimate by FH is based on applying pN self-force estimates to strong-field orbits, a regime where pN approximations are generally inaccurate. It is thus of great interest to estimate the impact of orbital resonances using strong-field methods. The purpose of this paper is to take a first step in this direction.

Our goal is to generalize our computational techniques in order to treat resonances correctly. A key point is that the flux-balancing technique which can be used to approximate inspiral (as described in the final paragraph of Sec. I A) is based on the adiabatic approximation. This approximation temporarily breaks down during a resonance. Therefore, to treat resonances, one must use the orbital equations of motion (1.1–1.2) to track the evolution of all the orbital degrees of freedom on short time scales. Flux balancing instead just tracks the evolution of the conserved quantities E, L_z, and Q on long time scales. In addition one must use the full, oscillatory self-force driving term $G_i^{(1)}$, and not just its averaged version.

As is well known, computation of the full self-force is extremely difficult, largely because it requires regularization of the self-field [7]. Fortunately, only the dissipative piece of the self-force should contribute to leading order resonance effects. As argued in FH, there is some evidence suggesting that geodesic motion perturbed by the conservative piece of the self-force is an integrable dynamical system, and resonances do not occur in such systems. Thus, if the integrability conjecture of FH is true, only the dissipative self-force needs to be computed. This constitutes a great simplification, since the well-known difficulties of self-force computations apply only to the conservative piece; the dissipative piece is relatively straightforward to compute. Techniques for doing so with scalar fields were presented in Ref. [21], and generalizing to the gravitational dissipative self-force is not terribly difficult [14,15]. While these references focused on the *averaged* self-force, it is straightforward to generalize the analysis to obtain the full dissipative self-force.

It is thus feasible to perform numerical compututations of orbital evolutions through resonances using the full dissipative self-force, without any orbit averaging. Our eventual goal is to extend our black hole perturbation theory codes to do just this, and to evaluate how the dissipative self-force behaves as a system evolves through resonance. Work in this vein is in progress and will be presented in future work [39].

In this paper, we take a first step in this direction. We focus here on computation of time-averaged fluxes of the integrals of the motion, and in particular on how these quantities differ between resonant and nonresonant orbits. These quantities correspond to the fluxes that one would measure at infinity (and at the black hole horizon) if one turned off radiation reaction effects; upon averaging over long times, they are equal to the rate at which the dissipative self-force evolves these constants. We emphasize that these quantities are not sufficient to allow computation of orbital evolutions. However, they provide insight into the characteristic features of the radiation emitted by resonant orbits.

We find that fluxes from resonant orbits generically differ from those from nearby, nonresonant orbits,[1] and in addition vary depending on the relative phase of the radial and angular motions. The magnitude of this variation is closely related to the "kick" that is imparted to the orbit's constants as it evolves through a resonance (cf. Fig. 1 of FH). As such, characterizing on-resonance fluxes is a useful and natural first step in the process of modifying existing flux-based codes to compute the full dissipative self-force. We explore numerically the magnitude of the difference between the resonant and nonresonant cases, and the dependence on the orbital phase. For specific modes, the fluxes can vary by large factors (although variations of order unity are more typical). For the net fluxes obtained by summing over all modes, variations are typically of order a percent or less.

D. Outline of this paper

We begin this paper by briefly reviewing the behavior of Kerr geodesic orbits in Sec. II. Much of this material has been presented elsewhere, so we leave out most details, pointing the reader to appropriate references. Our main focus is to describe how to find and characterize resonant orbits. We then describe how to compute radiation from Kerr orbits in Sec. III. We first briefly review the Teukolsky-equation-based formalism we use (Secs. III A–III B), and then describe how key details are modified by

[1]Thus the fluxes change discontinuously as one varies the orbital parameters. This is certainly unphysical, but arises because we compute infinite time averages of fluxes from geodesic orbits. If one considers the fluxes from the true inspiraling motion, and averages over a time scale intermediate between the orbital time scale and the radiation reaction time scale, the time-averaged fluxes would vary smoothly with time, with order unity changes in the vicinity of resonances. This point is discussed further in Appendix B.

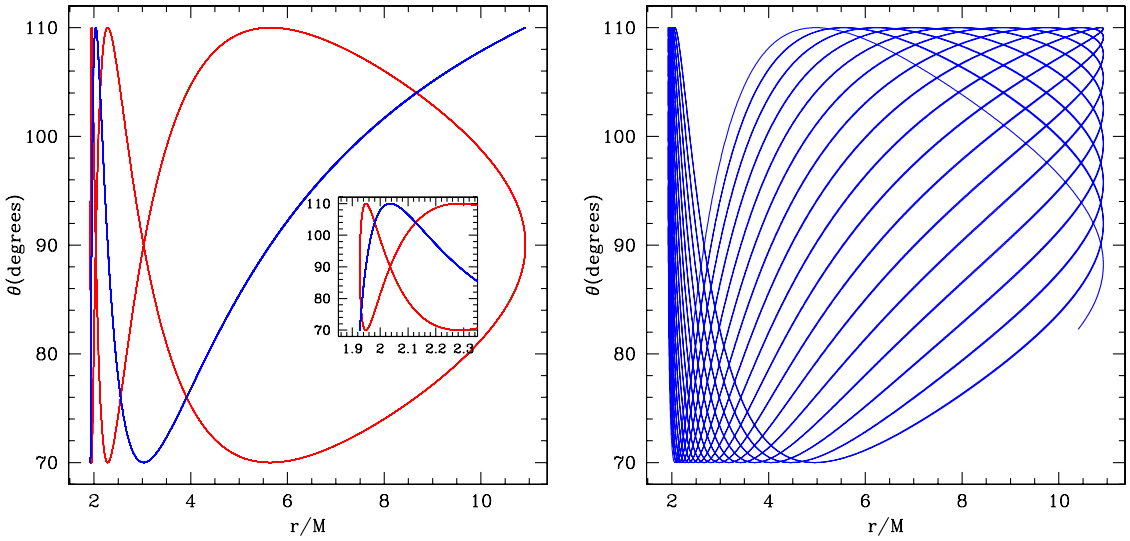

FIG. 1 (color online). Left: Lissajous figures describing motion in the (r, θ) plane on a 3:1 orbital resonance ($a = 0.9M$, $p = 3.2758M$, $e = 0.7$, $\theta_m = 70°$). The blue trace has $\theta = \theta_m$ at periapsis; red has $\theta = \pi/2$ at periapsis. The inset image zooms in on the region $1.9M \lesssim r \lesssim 2.3M$, clarifying the angular oscillation at very small radius. Approximately nine radial cycles are used to generate these traces. Right: Ergodic motion of a "normal" orbit. The orbit's geometry is identical to that in the left-hand panel, but we have changed the black hole's spin to $a = 0.95M$; this changes the ratio of frequencies to $\Omega_\theta/\Omega_r = 2.0311\ldots$. Again, roughly nine radial cycles are shown here. Given enough time, this trace would pass arbitrarily close to all points in $70° \leq \theta \leq 110°$, $2M \lesssim r \lesssim 12M$.

orbital resonances in Secs. III C and III D. We describe two complementary approaches to computing fluxes on resonance. Although formally equivalent (as we prove in Appendix A), their implementation is quite different. Having both methods at hand proved useful to us in our numerical study. One aspect of the on-resonance computation (the evolution of Carter's constant Q) is sufficiently complicated that all details of this calculation are given in Appendix B. Our analytic results for fluxes of energy and angular momentum on resonance agree with those obtained by Grossman, Levin, and Perez-Giz (compare especially & Secs. III D–E and Appendices B5, B6, and C in Ref. [18] with our discussion here, and with our Appendix A). Our result for the resonant rate of change of the Carter constant appears to be new.

Our numerical results are given in Sec. IV. We begin by examining how fluxes from individual modes (i.e., harmonics of the orbital frequencies) behave as a function of the offset phase of the radial and angular motions, which we denote χ_0. We show that the amplitude of a given mode, and hence the rates of change of conserved quantities associated with that mode, can vary significantly with χ_0. For example, the flux of energy from an orbit can vary by factors of order unity as χ_0 varies from 0 to 2π. The rate of change of the orbit's Carter constant can even change sign as χ_0 varies. The total flux from a given orbit is given, however, by adding fluxes from many modes. When many modes are combined, much of the variation washes away; we find variations of a fraction of a percent in most quantities after summation. The amount of this residual variation seems to depend most strongly upon the geometry of the orbit's (r, θ) motion on resonance, in particular, the topology of the trace in the (r, θ) plane. Orbits whose motion in (r, θ) have a simple topology with few trajectory crossings in the plane (e.g., the $\Omega_\theta/\Omega_r = 3/2$ resonance) tend to have a relatively large variation in the integrals of motion; orbits whose motion has a more complicated topology with many trajectory crossings show much less variation (e.g., the $\Omega_\theta/\Omega_r = 4/3$ resonance). We argue that this can be explained in terms of how the orbital motion tends (or fails) to average away variations in the source term to the Teukolsky equation.

As emphasized in Sec. I C, understanding these fluxes exactly on resonance is only the first step in building a complete strong-field understanding of how resonances impact inspirals. In particular, these results do not provide enough information to specify how a system will evolve through a resonance. To go further, it will be necessary to examine how dissipation behaves as the system evolves toward and through an orbital resonance. As mentioned above, this analysis is now beginning; we briefly outline the approach we are pursuing in Sec. V.

Throughout this paper, we use "relativist's units," setting $G = 1 = c$.

II. KERR GEODESICS AND ORBITAL RESONANCES

A. Brief summary of general characteristics

We begin by reviewing geodesic orbits of Kerr black holes, with a focus on aspects of this motion particularly relevant to our analysis. In most textbooks [for example,

Ref. [27], Eqs. (33.32a)–(33.32d)], Kerr geodesics for a massive body are described using equations of motion in the Boyer-Lindquist coordinates t, r, θ, and ϕ:

$$\Sigma^2\left(\frac{dr}{d\tau}\right)^2 = [E(r^2+a^2) - aL_z]^2 - \Delta[r^2 + (L_z - aE)^2 + Q] \equiv R(r), \tag{2.1}$$

$$\Sigma^2\left(\frac{d\theta}{d\tau}\right)^2 = Q - \cot^2\theta L_z^2 - a^2\cos^2\theta(1-E^2) \equiv \Theta(\theta), \tag{2.2}$$

$$\Sigma\left(\frac{d\phi}{d\tau}\right) = \csc^2\theta L_z + aE\left(\frac{r^2+a^2}{\Delta} - 1\right) - \frac{a^2 L_z}{\Delta} \equiv \Phi(r,\theta), \tag{2.3}$$

$$\Sigma\left(\frac{dt}{d\tau}\right) = E\left[\frac{(r^2+a^2)^2}{\Delta} - a^2\sin^2\theta\right] + aL_z\left(1 - \frac{r^2+a^2}{\Delta}\right) \equiv T(r,\theta). \tag{2.4}$$

In these equations, τ is proper time along the geodesic, $\Sigma = r^2 + a^2\cos^2\theta$, and $\Delta = r^2 - 2Mr + a^2$. The quantities E and L_z are the orbital energy and axial angular momentum, normalized to the mass μ of the orbiting body, and Q is the orbit's Carter constant, normalized to μ^2. These three quantities are conserved on any geodesic.

Along with the coordinate time t and proper time τ, it is often very useful to work using a time parameter λ, defined by $d\lambda = d\tau/\Sigma$. The geodesic equations parametrized in this way are

$$\left(\frac{dr}{d\lambda}\right)^2 = R(r), \qquad \left(\frac{d\theta}{d\lambda}\right)^2 = \Theta(\theta), \qquad \frac{d\phi}{d\lambda} = \Phi(r,\theta), \qquad \frac{dt}{d\lambda} = T(r,\theta). \tag{2.5}$$

By using λ as our orbital parameter, the r and θ coordinate motions are completely separated from one another. Proper time τ couples r and θ by the factor Σ; the coupling with coordinate time t is even more complicated. The parameter λ is often called "Mino time," following Mino's use of it to untangle these coordinate motions [11].

We have found it useful for many of our studies to introduce the following reparametrization of r and θ:

$$r = \frac{pM}{1 + e\cos\psi}, \qquad \cos\theta = \cos\theta_m\cos(\chi + \chi_0). \tag{2.6}$$

These transformations replace the variables r and θ with secularly accumulating angles ψ and χ. As ψ and χ evolve from 0 to 2π, r and θ move through their full ranges of motion. We define $\chi = \psi = 0$ at $\lambda = 0$.

Notice that we include an offset phase χ_0 for the angular motion. We could also include an offset phase ψ_0 for the radial motion, as well as initial conditions ϕ_0 and t_0 for the ϕ and t coordinates. We choose our time origin such that $t = 0$ when $\lambda = 0$, which means $t_0 = 0$. We likewise choose $\phi_0 = 0$. Changing ϕ_0 is equivalent to rotating around the black hole's spin axis, and can have no effect on the flux of energy and angular momentum from the system (although it introduces a phase offset to the system's gravitational waves).

Finally, we choose $\psi_0 = 0$, which amounts to setting $\lambda = 0$ at a moment that the orbit passes through periapsis, $r = r_{\rm peri} = pM/(1+e)$. The offset phase χ_0 thus sets the value of θ at periapsis. Previous work (e.g., [23]) has typically used $\chi_0 = 0$ as well. The parameter set $(\psi_0, \chi_0, \phi_0, t_0)$ is equivalent to the set $(\lambda_0^r, \lambda_0^\theta, \phi_0, t_0)$ used in Ref. [21]. Following this reference, $\chi_0 = 0$ will label the "fiducial geodesic." We will use it as a reference geodesic for some of the calculations in Sec. III.

In their original form, Eqs. (2.1)–(2.4), Kerr orbits are parametrized (up to initial conditions) by the three conserved constants E, L_z, and Q. The reparametrization (2.6) maps those constants to parameters that describes an orbit's coordinate geometry: semilatus rectum p, eccentricity e, and minimum angle θ_m. These quantities are likewise conserved along a geodesic. Schmidt [28] provides closed-form expressions for converting between (E, L_z, Q) and (p, e, θ_m). Either the set (E, L_z, Q) or (p, e, θ_m), plus the relative phase χ_0, completely specifies a geodesic for our purposes here.

B. Orbital frequencies and resonances

Each orbit has a set[2] of frequencies describing its motions with respect to r, θ, and ϕ. The frequencies

$$\Omega_{r,\theta,\phi} = 2\pi/T_{r,\theta,\phi} \tag{2.7}$$

are conjugate to the periods[3] expressed in coordinate time t; the frequencies

$$\Upsilon_{r,\theta,\phi} = 2\pi/\Lambda_{r,\theta,\phi} \tag{2.8}$$

are conjugate to these periods in Mino time λ. These two frequencies are related by a factor Γ which describes the average increase in t per unit λ:

$$\Omega_{r,\theta,\phi} = \Upsilon_{r,\theta,\phi}/\Gamma. \tag{2.9}$$

[2]Interestingly, this set is *not* unique: There exists in the strong field geometrically distinct orbits (i.e., with different parameters p, e, θ_m) that have identical frequencies. See Ref. [29] for a detailed discussion.

[3]Describing the periods using Boyer-Lindquist time t is a bit complicated; $T_{r,\theta,\phi}$ really describes an averaged notion of the periods. See Refs. [28,30] for more detailed discussions.

Details of how to compute these frequencies given (E, L_z, Q) or (p, e, θ_m) are given in Refs. [30,31]. One could also define frequencies conjugate to proper time τ (see, e.g., Ref. [28] and discussion in Sec. I), but the Ω and Υ frequencies are sufficient for our purposes.

We next review how the qualitative features of the resonant orbits differ from those of generic orbits, as background to Sec. III below. A more detailed discussion can be found in Sec. II of Ref. [18]. As an example, we compare a typical orbit, for which the ratio Ω_θ/Ω_r is some irrational number, to a resonant orbit, for which $\Omega_\theta/\Omega_r = \beta_\theta/\beta_r$, where β_θ and β_r are small integers with no common factors. Figure 1 shows the motion of three orbits, projected into the (r, θ) plane. In all cases, we have chosen $p = 3.2758$, $e = 0.7$, $\theta_m = 70°$; the motion is thus bound to the range $1.93M \le r \le 10.9M$, $70° \le \theta \le 110°$. (See also Fig. 1 of Ref. [18], which is very similar, although it does not illustrate the impact of the offset phase between the r and θ motions.)

In the right-hand panel, we have set the spin parameter $a = 0.95M$. For these orbital parameters, this orbit has $\Omega_\theta/\Omega_r = 2.0311\ldots$. This is *not* a resonant orbit; notice that the roughly nine radial periods shown here do not close. The orbital trace in this case ergodically fills the (r, θ) plane. In the left-hand panel, we have set $a = 0.9M$, which yields $\Omega_\theta/\Omega_r = 3$—these orbits are in a 3:1 resonance. The two traces shown in this panel correspond to different choices of χ_0. The blue trace has $\chi_0 = 0$ (so that $\theta = \theta_m = 70°$ at periapsis), and the red trace has $\chi_0 = \pi/2$ (so that $\theta = 90°$ at periapsis). Both traces show roughly nine complete radial periods. By their periodic nature, their motions trace out Lissajous figures: No matter how long we follow these orbits, they trace out a one-dimensional trajectory in the (r, θ) plane.

Note that the geometry of the traces in the left-hand panel varies significantly as χ_0 is varied. The topology of these traces remains fixed, however: In all cases the trace oscillates three times in the angular direction as it completes a single radial oscillation. As emphasized by Grossman *et al.* [17], the topology of resonant orbits is uniquely determined by their orbital parameters, by virtue of the integers β_θ and β_r that determine their periodicity. We show some evidence in Sec. IV that the topology of resonant orbits directly affects the strength of their resonance. Simple orbits, which do not cross themselves often and do not cover much of the allowed (r, θ) plane, show large variations in their radiated fluxes as the phase χ_0 is varied; more complicated orbits, which cross themselves many times and come close to much of the allowed (r, θ) plane, do not show such large variations.

III. GRAVITATIONAL RADIATION FROM KERR ORBITS

Here we describe in detail how we compute radiation from strong-field orbits, with an emphasis on how resonances modify the "usual" behavior. We begin in Sec. III A by briefly reviewing the Teukolsky equation and its solutions. This material has been presented at length in several other papers, so we only give a summary. Our goal is to provide just enough detail to understand how the situation changes on resonance. Section III B describes how to compute fluxes of energy E and angular momentum L_z from Teukolsky equation solutions, highlighting how this calculation must be modified for resonant orbits. The analogous calculation for the Carter constant calculation is sufficiently complicated that we present its details in Appendix B. Finally, Secs. III C and III D present two different ways to compute on-resonant fluxes. These methods are equivalent to one another, although their computational implementations are quite different. As mentioned in the Introduction, our analytic results for fluxes of E and L_z agree with those obtained in Ref. [18], while our results for the Carter constant are new.

A. The frequency-domain Teukolsky equation and its solutions

Our computation of the small body's self-interaction uses the Teukolsky equation [22]. This equation governs the radiative components to a Kerr black hole's spacetime curvature, ψ_0 and ψ_4, which arise due to some perturbing source or field. In the relevant limits, identities make it possible to obtain all information about the field ψ_0 from ψ_4, and vice versa, so we need only focus on one. The field ψ_4 is particularly convenient for describing radiation at infinity.

Teukolsky showed [22] that, imposing the Fourier and multipolar decomposition,

$$\psi_4 = \rho^4 \int_{-\infty}^{\infty} d\omega \sum_{lm} R_{lm\omega}(r) S_{lm\omega}(\theta) e^{i(m\phi - \omega t)}, \qquad (3.1)$$

where $\rho = -1/(r - ia\cos\theta)$, a master partial differential equation governing ψ_4 separates. The function $S_{lm\omega}(\theta)$ is a spin-weighted spheroidal harmonic; Ref. [32] presents techniques for computing it to high accuracy. The radial function is governed by

$$\Delta^2 \frac{d}{dr}\left(\frac{1}{\Delta}\frac{dR_{lm\omega}}{dr}\right) - V(r) R_{lm\omega} = -\mathcal{T}_{lm\omega}(r, \chi_0). \qquad (3.2)$$

Equation (3.2) is the Teukolsky equation (although that name is also used for the partial differential equation that governs ψ_4 before separating variables). Setting the right-hand side of (3.2) to zero, we construct a pair of homogeneous solutions, $R^H_{lm\omega}$ (which is regular on the event horizon) and $R^\infty_{lm\omega}$ (which is regular at infinity). See Ref. [23] (hereafter DH06) for a detailed discussion of how we construct these solutions, as well as for the potential $V(r)$ appearing in Eq. (3.2). From these solutions, it is straightforward to build a Green's function which can then be integrated over the source $\mathcal{T}_{lm\omega}$ to construct a particular solution.

The source $\mathcal{T}_{lm\omega}$ is sufficiently complicated that we will not write it out explicitly; see DH06 for details. It is built from projections of the stress-energy tensor for a small body orbiting the black hole,

$$T_{\alpha\beta} = \frac{\mu u_\alpha u_\beta}{\Sigma \sin\theta dt/d\tau}\delta[r - r_o(t)]\delta[\theta - \theta_o(t,\chi_0)]\delta[\phi - \phi_o(t)], \tag{3.3}$$

where μ is the mass of the small body, and u_α are the components of its orbital 4-velocity. The subscript "o" on the coordinates in the delta functions stands for "orbit," labeling the orbit's coordinates (as opposed to a general field point, which we leave without a subscript).

Note that $\mathcal{T}_{lm\omega}$ is a frequency-domain quantity. Because it arises from Kerr orbital motion, it only has support at frequencies $\omega_{mkn} = m\Omega_\phi + k\Omega_\theta + n\Omega_r$, and is nonzero only for $r_{\min} \le r \le r_{\max}$, $\theta_m \le \theta \le \pi - \theta_m$ [where $r_{\min} = p/(1+e)$, and $r_{\max} = p/(1-e)$; see Eq. (2.6)]. Once fully constructed, $\mathcal{T}_{lm\omega}$ has terms in $\delta[r - r_o(t)]$ and its first two radial derivatives; see Sec. III of DH06.

To understand fluxes from this system, our interest is in $R_{lm\omega}(r)$ in the limits $r \to \infty$ and $r \to r_+$ (the event horizon). These limits will allow us to deduce how the orbit evolves due to radiation to infinity, and due to radiation absorbed by the hole. As $r \to \infty$, the homogeneous solution $R^\infty_{lm\omega}(r)$ approaches (modulo a power-law scaling) an outgoing plane wave. Likewise, as $r \to r_+$, the solution $R^H_{lm\omega}(r)$ is limited to an ingoing plane wave. The particular solution we construct by integrating the Green's function over the source then takes the form

$$R_{lm\omega}(r) = \begin{cases} Z^H_{\omega lm}(\chi_0) R^\infty_{\omega lm}(r) & r \to \infty, \\ Z^\infty_{\omega lm}(\chi_0) R^H_{\omega lm}(r) & r \to r_+, \end{cases} \tag{3.4}$$

where

$$Z^\star_{lm\omega}(\chi_0) = C^\star \int_{r_+}^\infty dr' \frac{R^\star_{lm\omega}(r')\mathcal{T}_{lm\omega}(r',\chi_0)}{\Delta(r')^2}, \tag{3.5}$$

and where $\star$ can stand for ∞ or H. The symbol $C^\star$ is shorthand for a collection of constants whose value is not needed here; see Sec. III of DH06 for further discussion.

Next insert $\mathcal{T}_{lm\omega}$ into Eq. (3.5) and perform the r integral. The result is a Fourier transform:

$$\begin{aligned} Z^\star_{lm\omega}(\chi_0) &= C^\star \int_{-\infty}^\infty dt e^{i[\omega t - \phi(t)]} I^\star_{lm\omega}[r_o(t), \theta_o(t,\chi_0)] \\ &= C^\star \int_{-\infty}^\infty d\lambda e^{i(\omega\Gamma - m\Upsilon_\phi)\lambda} J^\star_{lm\omega}[r_o(\lambda), \theta_o(\lambda,\chi_0)]. \end{aligned} \tag{3.6}$$

The function $I^\star_{lm\omega}$ introduced on the first line of Eq. (3.6) is built from $\mathcal{T}_{lm\omega}$; see Eqs. (3.30)–(3.33) in DH06 and associated text for a detailed discussion. On the second line, we have changed the integration variable from coordinate time t to Mino time λ, and defined

$$\begin{aligned} J^\star_{lm\omega}(r_o,\theta_o) = I^\star_{lm\omega}(r_o,\theta_o) T(r_o,\theta_o) \\ \times e^{i[\omega\Delta t(r_o,\theta_o) - m\Delta\phi(r_o,\theta_o)]}. \end{aligned} \tag{3.7}$$

[In any place that we indicate a dependence on (r_o, θ_o), please note that this is shorthand for $[r_o(\lambda), \theta_o(\lambda,\chi_0)]$.] The function $J^\star_{lm\omega}(r_o,\theta_o)$ is just $I^\star_{lm\omega}(r_o,\theta_o)$ reweighted by $T(r_o,\theta_o)$ [the right-hand side of the geodesic equation (2.4)], and with the factor $e^{i(\omega\Delta t - m\Delta\phi)}$ included. The functions $\Delta t(r_o,\theta_o)$ and $\Delta\phi(r_o,\theta_o)$ are oscillatory contributions to the t and ϕ pieces of the orbit:

$$t_o(\lambda) = \Gamma\lambda + \Delta t[r_o(\lambda), \theta_o(\lambda,\chi_0)], \tag{3.8}$$

$$\phi_o(\lambda) = \Upsilon_\phi\lambda + \Delta\phi[r_o(\lambda), \theta_o(\lambda,\chi_0)]. \tag{3.9}$$

Both Δt and $\Delta\phi$ oscillate at harmonics of Υ_θ and Υ_r; see Ref. [30] for a detailed discussion.

The function $J^\star_{lm\omega}(r_o,\theta_o)$ gathers all the pieces of the integrand for $Z^\star_{lm\omega}$ that can be described as harmonics of Υ_θ and Υ_r. As such, it is useful to decompose it into these harmonics:

$$J^\star_{lm\omega}(r_o,\theta_o) = \sum_{kn} J^\star_{\omega lmkn}(\chi_0) e^{-i(k\Upsilon_\theta + n\Upsilon_r)\lambda}, \tag{3.10}$$

where

$$\begin{aligned} J^\star_{\omega lmkn}(\chi_0) = \frac{\Upsilon_r\Upsilon_\theta}{(2\pi)^2}\int_0^{2\pi/\Upsilon_\theta} d\lambda^\theta \int_0^{2\pi/\Upsilon_r} d\lambda^r \\ \times e^{i(k\Upsilon_\theta\lambda^\theta + n\Upsilon_r\lambda^r)} J^\star_{lm\omega}[r_o(\lambda^r), \theta_o(\lambda^\theta,\chi_0)]. \end{aligned} \tag{3.11}$$

We have here taken advantage of the fact that Mino time completely decouples the r and θ motions from one another. We imagine that these two coordinates depend separately on two different Mino-time variables, λ^r and λ^θ, and integrate over a full period of each time. See Ref. [30] for detailed discussion of this trick.

Next, combine Eqs. (3.6), (3.7), (3.10), and (3.11) to find

$$\begin{aligned} Z^\star_{lm\omega}(\chi_0) &= \frac{2\pi}{\Gamma}\sum_{kn} J^\star_{\omega lmkn}(\chi_0)\delta(\omega - \omega_{mkn}) \\ &\equiv \sum_{kn} Z^\star_{lmkn}(\chi_0)\delta(\omega - \omega_{mkn}). \end{aligned} \tag{3.12}$$

On the last line, we have taken advantage of the fact that the delta functions mean that the right-hand side only has support at $\omega = \omega_{mkn}$, and we have defined

$$Z^{\star}_{\omega lmkn}(\chi_0) = \frac{2\pi}{\Gamma} J^{\star}_{\omega lmkn}(\chi_0) = \frac{\Upsilon_r \Upsilon_\theta}{2\pi\Gamma} \int_0^{2\pi/\Upsilon_\theta} d\lambda^\theta \int_0^{2\pi/\Upsilon_r} d\lambda^r \tag{3.13}$$

$$e^{i(k\Upsilon_\theta \lambda^\theta + n\Upsilon_r \lambda^r)} J^{\star}_{lm\omega}[r_o(\lambda^r), \theta_o(\lambda^\theta, \chi_0)] \tag{3.14}$$

and

$$Z^{\star}_{lmkn}(\chi_0) = Z^{\star}_{\omega_{mkn} lmkn}(\chi_0). \tag{3.15}$$

Throughout this synopsis, we have explicitly shown the dependence on the relative phase χ_0. To account for its influence on the amplitudes, let us first define

$$\check{Z}^{\star}_{lmkn} \equiv Z^{\star}_{lmkn}(\chi_0 = 0). \tag{3.16}$$

In other words, amplitudes with a check mark $\check{}$ are computed using the fiducial geodesic. As shown in Sec. 8.4 of Ref. [21], the effect of χ_0 is to introduce a phase,

$$Z^{\star}_{lmkn}(\chi_0) = e^{i\xi_{mkn}(\chi_0)} \check{Z}^{\star}_{lmkn}, \tag{3.17}$$

where

$$\xi_{mkn}(\chi_0) = k\Upsilon_\theta \lambda^\theta_0 + m\Delta\hat{\phi}[r_{\min}, \theta(-\lambda^\theta_0)] - \omega_{mkn}\Delta\hat{t}[r_{\min}, \theta(-\lambda^\theta_0)], \tag{3.18}$$

where $\Delta\hat{\phi}$ is $\Delta\phi$ for the fiducial geodesic (and likewise for $\Delta\hat{t}$), and where $\lambda^\theta_0 = \lambda^\theta_0(\chi_0)$ is the value of λ^θ at which $\theta = \theta_m$. It is given explicitly by Eq. (3.75) of Ref. [21]. On the fiducial geodesic, $\lambda^\theta_0 = 0$, and $\xi_{mkn} = 0$, as it should.

B. The nonresonant rates of change of the orbital parameters E, L_z, and Q

As stated previously, our eventual goal is to compute the motion of a body which spirals through resonances under a rigorously computed self-force, or at least the dissipative piece of the self-force. The three components of the self-force can be regarded as the rates of change of the orbital constants E, L_z, Q. We will present results showing these rates of change for the dissipative self-force in a later paper. Here, we focus just on appropriately averaged rates of change of E, L_z, and Q.

In this section, we will show how to extract the rates at which gravitational radiation carries E and L_z to infinity and down the event horizon. This calculation has appeared many times in other papers; we present it in perhaps more detail than is necessary in order to highlight aspects of the calculation that change when we move from nonresonant to resonant orbits. One cannot extract the rate of change of Q from the radiation, but must instead compute it using the dissipative self-force. This is was done by Sago *et al.* [25] (hereafter S06). We go through the Sago *et al.* calculation in some detail in Appendix B in order to understand how to modify their result on an orbital resonance. In Appendix C, we likewise compute the rates of change of E and L_z using the dissipative self-force. The result we find there (for both resonant and nonresonant orbits) duplicates the rates of change we compute from gravitational-wave fluxes. This is not terribly surprising: Quinn and Wald [26] showed that this equality must hold given an appropriate averaging for these two ways of computing the evolution of E and L_z. Strictly speaking, Quinn and Wald's work does not apply to the situation we are studying—they do not consider black hole spacetimes (although they describe how to go beyond their calculation to include this limit) and require that the particle's trajectory begin and end far away from the gravitating source. Nonetheless, it demonstrates that this balance is to be expected in a wide range of situations, so the equality we find is sensible.

Using Eq. (3.1) and the definitions which follow, we find that as $r \to \infty$,

$$\psi_4 = \frac{1}{r} \sum_{lmkn} e^{i\xi_{mkn}(\chi_0)} \check{Z}^H_{lmkn} S_{lmkn}(\theta) e^{i(m\phi - \omega_{mkn} t)} \equiv \frac{1}{r} \sum_{lmkn} \psi_{4,lmkn}. \tag{3.19}$$

Here, $S_{lmkn}(\theta)$ is the spheroidal harmonic $S_{lm\omega}(\theta)$ for $\omega = \omega_{mkn}$. As $r \to \infty$, $\psi_4 \to (1/2)(\ddot{h}_+ - i\ddot{h}_\times)$, so

$$h_+ - ih_\times = -\frac{2}{r} \sum_{lmkn} \frac{\psi_{4,lmkn}}{\omega^2_{mkn}}. \tag{3.20}$$

A useful tool for understanding the energy carried by gravitational waves is the Isaacson stress-energy tensor [33], whose $r \to \infty$ limit is given by

$$T^{\rm rad}_{\mu\beta} = \frac{1}{16\pi} \langle \partial_\mu h_+ \partial_\beta h_+ + \partial_\mu h_\times \partial_\beta h_\times \rangle. \tag{3.21}$$

The angle brackets in this expression mean that the quantity is averaged over several wavelengths. See Ref. [33] and references therein for detailed discussion of the averaging procedure.

The energy flux, our focus here, is given by

$$\frac{dE^\infty}{dt} = \lim_{r\to\infty} r^2 \int T^{\rm rad}_{tk} n^k d\Omega = \lim_{r\to\infty} r^2 \int T^{\rm rad}_{tt} d\Omega, \tag{3.22}$$

where n^k is a radially outward pointing normal vector, and the index k is restricted to spatial directions.

Combining Eqs. (3.20)–(3.22)(3.22), we find

$$\left\langle \frac{dE^{\infty}}{dt} \right\rangle = \left\langle \sum_{lmkn} \sum_{l'm'k'n'} \mathrm{Re} \int \frac{\psi_{4,lmkn} \bar{\psi}_{4,l'm'k'n'}}{4\pi \omega_{mkn} \omega_{m'k'n'}} d\Omega \right\rangle; \tag{3.23}$$

$\bar{\psi}_4$ is the complex conjugate of ψ_4. The sum over l is taken from 2 to ∞; the sum over m from $-l$ to l; the sums over k and n are both taken from $-\infty$ to ∞; and likewise for the primed indices. The angle brackets on the left-hand side mean that this rate of change is to be understood as one which is averaged over appropriate orbital time scales.

Consider now averaging the right-hand side over several wavelengths. *Assuming that each frequency ω_{mkn} is distinct* (an assumption that is only true when we are not on a resonance), then this averaging forces $m = m'$, $k = k'$, $n = n'$. Using the fact that

$$\int S_{lmkn}(\theta) S_{l'mkn}(\theta) d\Omega = \delta_{ll'}, \tag{3.24}$$

we find

$$\left\langle \frac{dE^{\infty}}{dt} \right\rangle = \sum_{lmkn} \frac{|\check{Z}^{H}_{lmkn}|^2}{4\pi \omega^2_{mkn}} \equiv \sum_{lmkn} \dot{E}^{\infty}_{lmkn}. \tag{3.25}$$

A similar calculation focusing on $T^{\mathrm{rad}}_{t\phi}$ gives us the flux of axial angular momentum:

$$\left\langle \frac{dL^{\infty}_z}{dt} \right\rangle = \sum_{lmkn} \frac{m|\check{Z}^{H}_{lmkn}|^2}{4\pi \omega^3_{mkn}} \equiv \sum_{lmkn} \dot{L}^{\infty}_{z,lmkn}. \tag{3.26}$$

Notice that the phase ξ_{mkn} does not appear in Eqs. (3.25) and (3.26). Appendix C derives these results using the local self-force, following S06.

The calculation of fluxes down the horizon is more complicated. Since the Isaacson tensor is not defined in a black hole's strong field, we use the fact that the curvature perturbation from the orbiting body exerts a shear on the generators of the horizon, which increases the black hole's surface area. By the first law of black hole dynamics, this in turn changes its mass and angular momentum; see Refs. [34,35] for detailed discussions. Assuming flux balance, we can then read out the down-horizon fluxes:

$$\left\langle \frac{dE^{H}}{dt} \right\rangle = \sum_{lmkn} \alpha_{lmkn} \frac{|\check{Z}^{\infty}_{lmkn}|^2}{4\pi \omega^2_{mkn}} \equiv \sum_{lmkn} \dot{E}^{H}_{lmkn}, \tag{3.27}$$

$$\left\langle \frac{dL^{H}_z}{dt} \right\rangle = \sum_{lmkn} \alpha_{lmkn} \frac{m|\check{Z}^{\infty}_{lmkn}|^2}{4\pi \omega^3_{mkn}} \equiv \sum_{lmkn} \dot{L}^{H}_{z,lmkn}. \tag{3.28}$$

We refer the reader to Eq. (3.60) of DH06 for the down-horizon factor α_{lmkn}.

Unlike the energy and axial angular momentum, there is no simple formula describing the "flux" of the Carter constant carried by radiation. However, one can formulate how Q changes due to radiative backreaction. Taking into account only the dissipative piece of the self-force and averaging over very long times, Sago *et al.* [25] showed that

$$\left\langle \frac{dQ^{\infty}}{dt} \right\rangle = \sum_{lmkn} |\check{Z}^{H}_{lmkn}|^2 \times \frac{(\mathcal{L}_{mkn} + k\Upsilon_{\theta})}{2\pi \omega^3_{mkn}}, \tag{3.29}$$

$$\left\langle \frac{dQ^{H}}{dt} \right\rangle = \sum_{lmkn} \alpha_{lmkn} |\check{Z}^{\infty}_{lmkn}|^2 \times \frac{(\mathcal{L}_{mkn} + k\Upsilon_{\theta})}{2\pi \omega^3_{mkn}}, \tag{3.30}$$

where

$$\mathcal{L}_{mkn} = m\langle \cot^2\theta \rangle L_z - a^2 \omega_{mkn} \langle \cos^2\theta \rangle E. \tag{3.31}$$

It is interesting that the rate of change of Q can be factored into quantities that are encoded in the distant radiation ($\check{Z}^{H}_{lmkn}$ and $\check{Z}^{\infty}_{lmkn}$) and quantities that are local to the orbital worldline ($\mathcal{L}_{mkn}$, ω_{mkn}, and Υ_{θ}). Using Eqs. (3.25) and (3.27), these results can be written

$$\left\langle \frac{dQ^{\star}}{dt} \right\rangle = 2 \sum_{lmkn} \dot{E}^{\star}_{lmkn} \times (\mathcal{L}_{mkn} + k\Upsilon_{\theta})/\omega_{mkn}, \tag{3.32}$$

where $\star$ is either ∞ or H. We go through the Sago *et al.* calculation of $\langle dQ/dt \rangle$ in some detail in Appendix B in order to understand how to modify this result on an orbital resonance.

Note that the rates of change $\langle dE^{\star}/dt \rangle$, $\langle dL^{\star}_z/dt \rangle$, and $\langle dQ^{\star}/dt \rangle$ are equivalent for nonresonant orbits to the three components of the torus-averaged forcing term $\langle G^{(1)}_i \rangle$ introduced in the Introduction, albeit using coordinate time t rather than proper time τ to parametrize the rate of change. This equivalence breaks down for resonant orbits, as pointed out in Ref. [18].

C. Radiation from resonant orbits I: Merging of amplitudes on resonance

On resonance, $\Omega_{\theta}/\beta_{\theta} = \Omega_r/\beta_r \equiv \Omega$, and so $k\Omega_{\theta} + n\Omega_r = N\Omega$, where $N = k\beta_{\theta} + n\beta_r$. An infinite number of pairs (k, n) are consistent with a given N. For a given value of m, all pairs (k, n) satisfying $k\beta_{\theta} + n\beta_r = N$ will have mode frequency $\omega_{mkn} \equiv \omega_{mN} = m\Omega_{\phi} + N\Omega$.

Revisiting Eq. (3.19), this means that only three indices are needed to describe the radiation on resonance, rather than four:

$$\psi^{\mathrm{res}}_4 = \frac{1}{r} \sum_{lmN} \mathcal{Z}^{H}_{lmN}(\chi_0) S_{lmN}(\theta) e^{i(m\phi - \omega_{mN} t)}, \tag{3.33}$$

where

$$\mathcal{Z}^{\star}_{lmN}(\chi_0) = \sum_{(k,n)_N} e^{i\xi_{mkn}(\chi_0)} \check{Z}^{\star}_{lmkn}, \tag{3.34}$$

and where $(k,n)_N$ denotes all pairs $(k,\ n)$ which satisfy $k\beta_\theta + n\beta_r = N$. In Eq. (3.33), the sums over l and m are exactly as before, and N is summed from $-\infty$ to ∞. Equation (C16) of Ref. [18] gives a relationship, in their notation, that is equivalent to our Eq. (3.34).

Equations (3.33) and (3.34) tell us that, as we enter a resonance, modes of ψ_4 which were distinct combine with one another: "lines" in the gravitational-wave spectrum merge. Each mode's contribution to the combined amplitude (3.34) is weighted by its phase $\xi_{mkn}(\chi_0)$. Revisiting the calculation of the fluxes using Eq. (3.33) rather than (3.19), we find

$$\left\langle \frac{dE^{\infty}}{dt}(\chi_0) \right\rangle = \sum_{lmN} \frac{|\mathcal{Z}^{H}_{lmN}(\chi_0)|^2}{4\pi\omega^2_{mN}} \equiv \sum_{lmN} \dot{E}^{\infty}_{lmN}(\chi_0), \tag{3.35}$$

$$\left\langle \frac{dE^{H}}{dt}(\chi_0) \right\rangle = \sum_{lmN} \alpha_{lmN} \frac{|\mathcal{Z}^{\infty}_{lmN}(\chi_0)|^2}{4\pi\omega^2_{mN}} \equiv \sum_{lmN} \dot{E}^{H}_{lmN}(\chi_0), \tag{3.36}$$

$$\left\langle \frac{dL^{\infty}_z}{dt}(\chi_0) \right\rangle = \sum_{lmN} \frac{m|\mathcal{Z}^{\infty}_{lmN}(\chi_0)|^2}{4\pi\omega^3_{mN}} \equiv \sum_{lmN} \dot{L}^{\infty}_{z,lmN}(\chi_0), \tag{3.37}$$

$$\left\langle \frac{dL^{H}_z}{dt}(\chi_0) \right\rangle = \sum_{lmN} \alpha_{lmN} \frac{m|\mathcal{Z}^{\infty}_{lmN}(\chi_0)|^2}{4\pi\omega^3_{mN}} \equiv \sum_{lmN} \dot{L}^{H}_{z,lmN}(\chi_0). \tag{3.38}$$

(The factor α_{lmN} appearing here is the same as α_{lmkn} introduced earlier, but with ω_{mkn} replaced by ω_{mN}.) Thanks to the dependence of $\mathcal{Z}^{\star}_{lmN}$ on the relative phase χ_0, the on-resonance fluxes likewise depend on this phase. These equations reproduce Eq. (C15) of Ref. [18]. We derive them using the local self-force in Appendix C.

In Appendix B, we show how the calculation of dQ/dt is changed due to an orbital resonance. The result is

$$\left\langle \frac{dQ^{\infty}}{dt}(\chi_0) \right\rangle = \sum_{lmN} \frac{|\mathcal{Z}^{H}_{lmN}(\chi_0)|^2}{2\pi\omega^3_{mN}} \mathcal{L}_{mN} + \Upsilon_\theta \sum_{lmN} \frac{\mathrm{Re}[\mathcal{Z}^{H}_{lmN}(\chi_0)\bar{\mathcal{Y}}^{H}_{lmN}(\chi_0)]}{2\pi\omega^3_{mN}}, \tag{3.39}$$

$$\left\langle \frac{dQ^{H}}{dt}(\chi_0) \right\rangle = \sum_{lmN} \frac{\alpha_{lmN}|\mathcal{Z}^{\infty}_{lmN}(\chi_0)|^2}{2\pi\omega^3_{mN}} \mathcal{L}_{mN} + \Upsilon_\theta \sum_{lmN} \frac{\alpha_{lmN}\mathrm{Re}[\mathcal{Z}^{\infty}_{lmN}(\chi_0)\bar{\mathcal{Y}}^{\infty}_{lmN}(\chi_0)]}{2\pi\omega^3_{mN}}. \tag{3.40}$$

The factor $\mathcal{L}_{mN}$ is the same as $\mathcal{L}_{mkn}$ with ω_{mkn} replaced by ω_{mN}. We have introduced the modified amplitude

$$\mathcal{Y}^{\star}_{lmN}(\chi_0) = \sum_{(k,n)_N} k e^{i\xi_{mkn}(\chi_0)} \check{Z}^{\star}_{lmkn}. \tag{3.41}$$

Notice that $\mathcal{Y}^{\star}_{lmN}(\chi_0)$ is similar to $\mathcal{Z}^{\star}_{lmN}(\chi_0)$ [compare Eq. (3.34)], but with each term in the sum weighted by k. Equations (3.39) and (3.40) are used in the following section to study how the Carter constant's evolution is affected by an orbital resonance.

D. Radiation from resonant orbits II: The constrained source integral of a resonant orbit

The method described in Sec. III C builds the on-resonance amplitudes $\mathcal{Z}^{\star}_{lmN}(\chi_0)$ from the amplitudes $\check{Z}^{\star}_{lmkn}$ which are normally computed with frequency-domain Teukolsky equation solvers, such as that described in DH06. The only modification is the need to compute the phase $\xi_{mkn}(\chi_0)$.

One can also compute the on-resonant amplitudes by modifying the integral for the amplitudes $\check{Z}^{\star}_{lmkn}$. Doing so, we compute $\mathcal{Z}^{\star}_{lmN}(\chi_0)$ directly, without reference to the amplitudes $\check{Z}^{\star}_{lmkn}$. We begin this calculation by carrying over without modification the computation of Sec. III A up to Eq. (3.6),

$$Z^{\star}_{lm\omega} = C^{\star} \int_{-\infty}^{\infty} d\lambda e^{i(\omega\Gamma - m\Upsilon_\phi)\lambda} J^{\star}_{lm\omega}[r_o(\lambda), \theta_o(\lambda, \chi_0)].$$

As before, we decompose $J^{\star}_{lm\omega}$ into Υ_θ and Υ_r harmonics. However, we now take into account how these frequencies are related on a resonance:

$$J^{\star}_{lm\omega} = \sum_{kn} J^{\star}_{\omega lmkn} e^{-i(k\Upsilon_\theta + n\Upsilon_r)\lambda} = \sum_{kn} J^{\star}_{\omega lmkn} e^{-i(k\beta_\theta + n\beta_r)\Upsilon\lambda} \equiv \sum_{N} \mathcal{J}^{\star}_{\omega lmN} e^{-iN\Upsilon\lambda}. \tag{3.42}$$

On the second line, we have used the resonance relation $\Upsilon_\theta/\beta_\theta = \Upsilon_r/\beta_r \equiv \Upsilon$. We then use $N = k\beta_\theta + n\beta_r$, and change notation slightly to distinguish the source amplitude $J^{\star}_{\omega lmkn}$ from its on-resonance variant $\mathcal{J}^{\star}_{\omega lmN}$.

The result, Eq. (3.42), depends on only one fundamental frequency, Υ. As such, our integral for $\mathcal{J}^{\star}_{\omega lmN}$ is taken over only a single time variable λ:

$$\mathcal{J}^{\star}_{\omega lmN}(\chi_0) = \frac{\Upsilon}{2\pi}\int_0^{2\pi/\Upsilon} d\lambda J^{\star}_{lm\omega}[r_o(\lambda),\theta_o(\lambda,\chi_0)]e^{iN\Upsilon\lambda}. \tag{3.43}$$

Finally, by combining Eqs. (3.6), (3.7), (3.42), and (3.43), we define

$$\mathcal{Z}^{\star}_{lmN}(\chi_0) = \frac{2\pi}{\Gamma}\mathcal{J}^{\star}_{\omega_{mN}lmN}(\chi_0) \tag{3.44}$$

$$= \frac{\Upsilon}{\Gamma}\int_0^{2\pi/\Upsilon} d\lambda J^{\star}_{lm\omega_{mN}}[r(\lambda),\theta(\lambda,\chi_0)]e^{iN\Upsilon\lambda}. \tag{3.45}$$

Equation (B33) of Ref. [18] is equivalent to Eq. (3.45) here.

In combining the previous relations to derive Eq. (3.45), we find a proportionality to $\delta(\omega-\omega_{mN})$, which forces the right-hand side to have support only at $\omega=\omega_{mN}$. Although it may not be obvious, Eqs. (3.34) and (3.45) are equivalent. We show this analytically in Appendix A, and will demonstrate it numerically in the following section. A conceptually attractive feature of Eq. (3.45) is that the integrand is only evaluated at the coordinates (r,θ) which the on-resonance orbit passes through. Changing χ_0 changes the points (r,θ) at which the integrand has support. This is how the dependence on χ_0 enters $\mathcal{Z}^{\star}_{lmN}$ in this calculation.

However, Eq. (3.45) can only be used for orbits that are *exactly* on resonance. Indeed, in any other case, the 3-index amplitude $\mathcal{Z}^{\star}_{lmN}$ is not meaningful since the on-resonance condition $k\beta_\theta + n\beta_r = N$ is not met. A suitable generalization of Eq. (3.34) for slightly off-resonance orbits can be used to understand the behavior of ψ_4 as one approaches and moves through a resonance. As such, the sum of phase-weighted amplitudes, Eq. (3.34), is likely to be more useful for understanding the resonant self interaction in full inspiral studies. In any case, we have found having two techniques for computing $\mathcal{Z}^{\star}_{lmN}(\chi_0)$ to be very useful. The codes which implement these two formulas are quite different, so it is reassuring that their results are in agreement. As discussed at the end of Appendix B, it appears that the modified amplitude $\mathcal{Y}_{lmN}(\chi_0)$ can also be computed with a one-dimensional integral by propagating the operator $(d\theta/d\lambda)\partial_\theta$ under the integral in Eq. (3.45). We have not yet tested this, though it would be a worthwhile exercise to do so.

IV. RESULTS: HOW RESONANCES IMPACT RADIATION

A. Variation of modes with χ_0 and comparison of two computational techniques

We now discuss examples illustrating how wave amplitudes and fluxes are affected by orbital resonances. All of our results are computed using a version of the code described in DH06, modified to handle resonances.

Begin with Fig. 2, which illustrates how $\mathcal{Z}^{H}_{lmN}$ and $\mathcal{Z}^{\infty}_{lmN}$ behave as functions of χ_0. For this example, we have put $a=0.9M$, $p=8.7744M$, $e=0.7$, $\theta_m=20^\circ$ (for

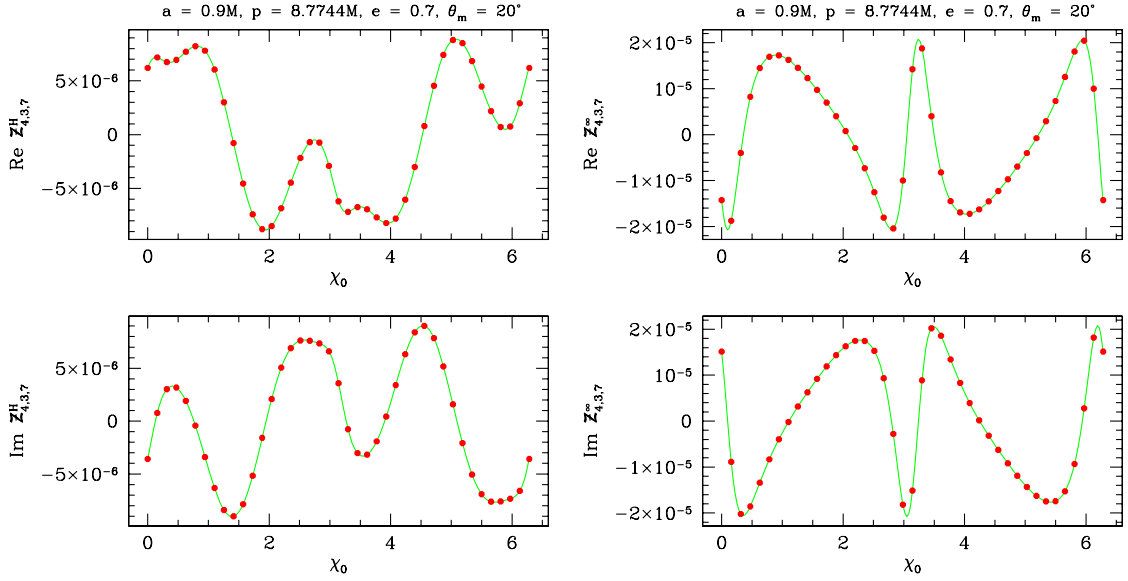

FIG. 2 (color online). Comparison of two methods to compute the on-resonance amplitudes $\mathcal{Z}^{\star}_{lmN}$. All panels correspond to radiation from an orbit with parameters $p=8.7744M$, $e=0.7$, $\theta_m=20°$, about a black hole with spin $a=0.9M$. For this orbit, $\Omega_\theta/\Omega_r=3/2$. We have chosen $l=4$, $m=3$, $N=7$. Left panels show $\mathcal{Z}^{H}_{437}$, right panels show $\mathcal{Z}^{\infty}_{437}$; top panels show the real part, bottom panels the imaginary part. Blue curves show the amplitude computed by the on-resonance merging of amplitudes discussed in Sec. III C; red dots show the amplitude computed using the constrained source integral presented in Sec. III D. The two methods agree to numerical accuracy (roughly 6 digits in this case).

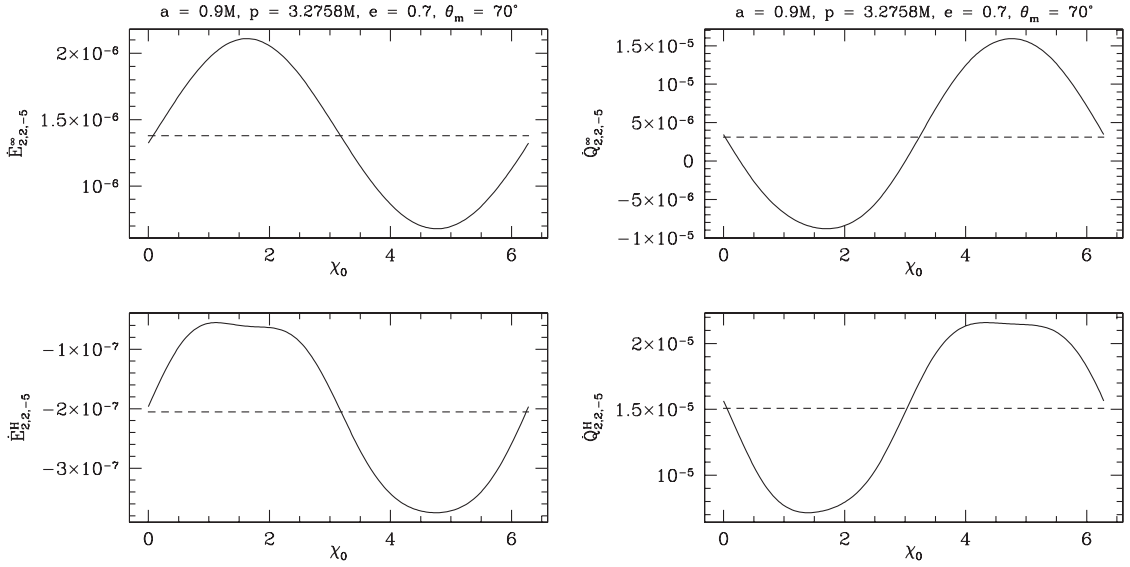

FIG. 3. On-resonance variation of the rates of change of orbital energy (left panels) and Carter constant (right panels) in the $l = 2$, $m = 2, N = -5$ mode for an orbit with $p = 3.2758M$, $e = 0.7, \theta_m = 70°$, $a = 0.9M$ (for which $\Omega_\theta/\Omega_r = 3$). Top panels give the flux to infinity, bottom ones give flux down the horizon. The dashed line in all panels shows the value that would be obtained if the resonance were neglected (i.e., simply adding in quadrature the various 4-index amplitudes $Z^\star_{lmkn}$ that contribute to the 3-index amplitude $\mathcal{Z}^\star_{lmN}$). In all cases, the flux varies considerably with the phase χ_0. The variation in $\dot{Q}^\infty$ is especially interesting in this case, changing sign at $\chi_0 \simeq 0.28$ and $\chi_0 \simeq 3.01$. We do not show $\dot{L}^\star_z(\chi_0)$ for this mode, since it is identical to $\dot{E}^\star(\chi_0)$ modulo a factor of m/ω_{mN}.

which $\Omega_\theta/\Omega_r = 3/2$), and we have chosen $l = 4$, $m = 3$, $N = 7$. In all panels, the green curves show $\mathcal{Z}^\star_{lmN}$ computed using Eq. (3.34); the red dots show the same quantity computed using Eq. (3.45). The two methods agree to numerical accuracy (roughly 6 digits[4]). All examples that we have examined show that Eqs. (3.34) and (3.45) agree perfectly (as we would expect from the calculation presented in Appendix A). Having both methods at hand was quite useful for debugging the on-resonance version of our code.

Besides showing the excellent agreement between our methods of computing $\mathcal{Z}^\star_{lmN}$, Fig. 2 also illustrates how $\mathcal{Z}^\star_{lmN}$ varies with χ_0. For this example, we find that $|\mathcal{Z}^H_{lmN}|$ varies by about 25% from minimum to maximum, and $|\mathcal{Z}^\infty_{lmN}|$ varies by about 40%. The associated energy fluxes, which are proportional to the amplitude's modulus squared, varies by about 55% and by a factor of 2, respectively.

Figures 3 and 4 give two examples of the on-resonance rate of change of orbital constants. We show $\dot{E}^\star_{lmN}$ and $\dot{Q}^\star_{lmN}$ for two orbits about a black hole with $a = 0.9$. Figure 3 shows the $l = 2$, $m = 2$, $N = -5$ mode computed for an orbit with $p = 3.2758M$, $e = 0.7$, $\theta_m = 70°$; in this case, $\Omega_\theta/\Omega_r = 3$. Figure 4 shows the $l = 5$, $m = -2$, $N = 11$ mode for an orbit with $p = 4.5322M$, $e = 0.3$, $\theta_m = 45°$, for which $\Omega_\theta/\Omega_r = 2$.

[4]It is not difficult to do the calculations more accurately than this [36–38], but 6 digits of accuracy is good enough for this first strong-field examination of this effect.

In both cases, the flux of energy to infinity varies by a factor of about 3.1. This agreement is a coincidence. The down-horizon flux shows more variety, varying by a factor of about 6.8 for the 3:1 resonance, and by a factor of nearly 10^3 for the 2:1 case. (This large variation is because the flux comes close to zero at $\chi_0 \simeq 4.7$.) The variation in $\dot{Q}^\infty_{2,2,-5}$ is especially interesting for the 3:1 resonance: It is negative over nearly half the span of χ_0, but is positive elsewhere. This behavior is unique to the on-resonance form of $\dot{Q}^\star_{lmN}$, and arises from the fact that it contains a term proportional to $\mathrm{Re}[\mathcal{Z}_{lmN}\bar{\mathcal{Y}}_{lmN}]$. Because the amplitudes $\mathcal{Z}_{lmN}$ and $\mathcal{Y}_{lmN}$ can have different phases, the behavior of $\dot{Q}^\star_{lmN}$ can be more complicated than the behavior of the energy or angular momentum fluxes. Those fluxes are both proportional to $|\mathcal{Z}^\star_{lmN}|^2$, and hence are positive or negative definite.

The horizontal dashed lines in these figures gives the rate of change that would be found if the resonance were neglected. In other words, it shows the rate of change one would find by simply combining in quadrature all of the 4-index amplitudes $Z^\star_{lmkn}$ which contribute to the relevant 3-index amplitude $\mathcal{Z}^\star_{lmN}(\chi_0)$. Its value is the average with respect to λ^θ_0 of the resonant flux:

$$\dot{E}^{\star,\text{no-res}}_{lmN} = \frac{\Upsilon_\theta}{2\pi}\int_0^{2\pi/\Upsilon_\theta} \dot{E}^\star_{lmN} d\lambda^\theta_0 = \frac{\Upsilon_\theta}{2\pi}\int_0^{2\pi} \dot{E}^\star_{lmN}(\chi_0)\frac{d\lambda^\theta_0}{d\chi_0}d\chi_0. \quad (4.1)$$

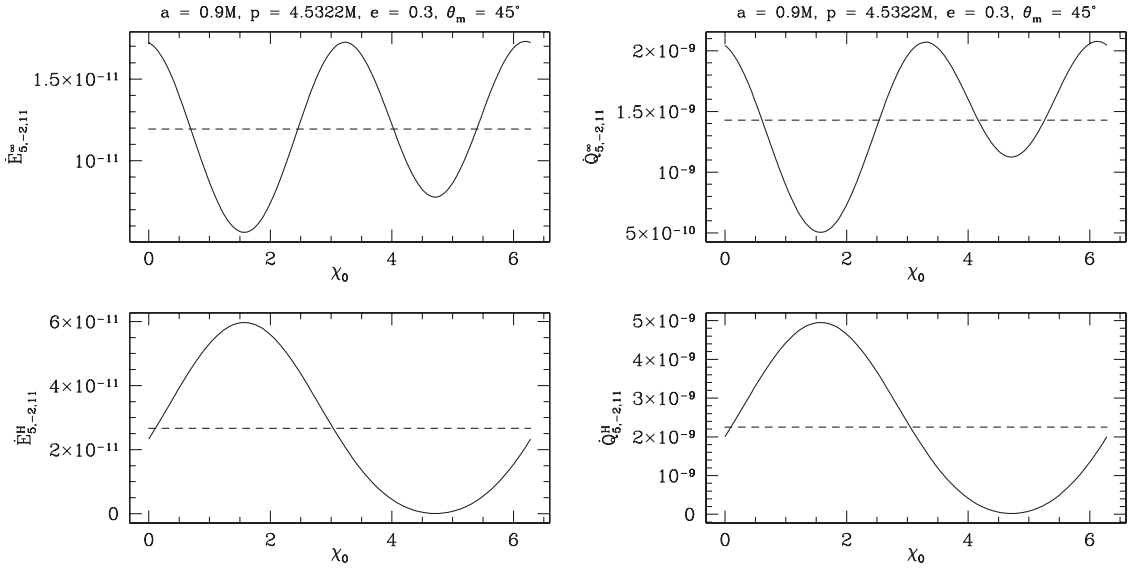

FIG. 4. On-resonance variation of the rates of change of orbital energy (left panels) and Carter constant (right panels) in the $l = 5$, $m = -2$, $N = 11$ mode for an orbit with $p = 4.5322M$, $e = 0.3$, $\theta_m = 45°$, $a = 0.9M$ (for which $\Omega_\theta/\Omega_r = 2$). Top panels give the flux to infinity, bottom ones give flux down the horizon. The dashed line gives the value found when the resonance is neglected. As in Fig. 3, we see that $\dot{E}^\star_{lmN}$ and $\dot{Q}^\star_{lmN}$ vary quite a bit as χ_0 sweeps from 0 to 2π, with minima near zero in this case for the down-horizon quantities.

Recall that the parameter λ^θ_0, introduced in Eq. (3.18), sets the value of λ^θ at which $\theta = \theta_m$. An explicit expression for the Jacobian $d\lambda^\theta_0/d\chi_0$ is given in Eq. (3.76) of Ref. [21]. It is not difficult to show that this result must hold[5]: combining Eqs. (3.34) and (3.35), we have

$$\dot{E}^\infty_{lmN}(\chi_0) = \frac{1}{4\pi\omega^2_{mN}}\left(\sum |\check{Z}^H_{lmkn}|^2 + \sum \check{Z}^H_{lmkn}\bar{\check{Z}}^H_{lmk'n'} e^{i[\xi_{mkn}(\chi_0)-\xi_{mk'n'}(\chi_0)]}\right). \quad (4.2)$$

The first sum in this expression is, as usual, taken over all pairs $(k,n)_N$, as defined earlier. The second sum is taken over the pair of pairs $(k,n)_N$ and $(k',n')_N$, with $k \neq k'$, $n \neq n'$. The first sum is exactly $\dot{E}^{\infty,\text{no-res}}_{lmN}$. Using Eq. (3.18), we see that on resonance,

$$\xi_{mkn} - \xi_{mk'n'} = (k-k')\Upsilon^\theta\lambda^\theta_0. \quad (4.3)$$

Hence this term averages to zero, demonstrating the validity of Eq. (4.1). Similar results hold for all of the other rates of change we compute in this paper. An alternative demonstration of the identity (4.1) in a more general context can be found in Appendix C2 of Ref. [18].

These examples show that the flux carried in each mode can vary significantly as a function of χ_0. This shows that in principle resonances can have a strong impact on gravitational-wave fluxes. Notice, though, that the detailed dependence of each mode on χ_0 varies quite a bit from mode to mode. It would not be surprising if much of the variation cancels out after summing over many modes. We examine this in the next section, checking to see how much flux variation remains when many modes are added.

B. Sum over many modes: Variation of total flux

We now examine the variation in total flux on resonant orbits, computing the sums (3.35) and (3.36). Those sums are taken over an infinite number of modes, which we cannot do in a numerical calculation. We instead truncate the sum over index l at $l_{\max} = 6$; for orbits with $e = 0.3$, we truncate the sum over N at $N_{\max} = 50$, and truncate at $N_{\max} = 100$ for $e = 0.7$:

$$\dot{E}^\star(\chi_0) = \sum_{l=2}^{l_{\max}} \sum_{m=-l}^{l} \sum_{N=-N_{\max}}^{N_{\max}} \dot{E}^\star_{lmN}(\chi_0). \quad (4.4)$$

We have not performed a careful convergence analysis, but we have found that increasing $l_{\max}$ and $N_{\max}$ only changes our numerical results by an unimportant fraction for the orbits we have examined so far. We do not claim our accuracy to be good enough for "production" purposes, but we do claim it is good enough to illustrate the physics that we present here.

Figure 5 shows one example of how, after summing over many modes, $\dot{E}^\star$ varies as a function of χ_0. We put $a = 0.9M$, and choose an orbit with $p = 5.48622M$, $e = 0.7$, and $\theta_m = 70°$, for which $\Omega_\theta/\Omega_r = 3/2$. The fractional variation in $\dot{E}^\star$ we find is much smaller than

[5]At one point in our analysis, preliminary results indicated that averages did not respect Eq. (4.1). Gabriel Perez-Giz insisted to one of us (S. A. H.) that this must be an error. Indeed, these preliminary results were wrong.

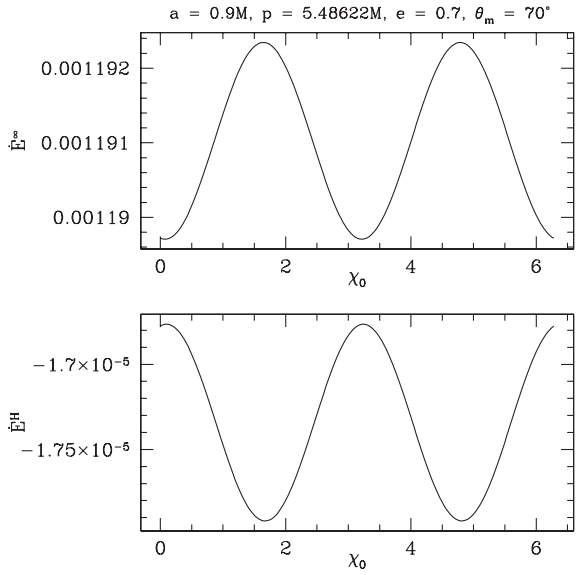

FIG. 5. Variation of total energy flux, both to infinity (top) and down the horizon (bottom) for an orbit with $p = 5.48622M$, $e = 0.7$, $\theta_m = 70°$, $a = 0.9M$ (for which $\Omega_\theta/\Omega_r = 3/2$). After summing over many modes, the variation is significantly reduced: the flux to infinity only varies by about 0.127%, and that down the horizon varies by roughly 1.6%. The variations in $\dot{L}_z^\star(\chi_0)$ and $\dot{Q}^\star(\chi_0)$ are qualitatively similar, so we do not show them. See Table II for more details.

the variation we saw in individual modes: the summed flux to infinity varies by about 0.2%, and the down-horizon flux varies by about 6.7%. The down-horizon flux is much smaller than the flux to infinity, so the variations are dominated by the behavior of $\dot{E}^\infty$. The behaviors of $\dot{L}_z^\star(\chi_0)$ and $\dot{Q}^\star(\chi_0)$ are qualitatively similar to $\dot{E}^\star(\chi_0)$, so we do not show plots for those quantities.

Tables I–IV present the fractional variation in $\dot{E}^\star$, $\dot{L}_z^\star$, and $\dot{Q}^\star$ for several orbits about a black hole with spin $a = 0.9M$. Within each table, we fix e and θ_m. We look at large and small eccentricity ($e = 0.7$ and $e = 0.3$), and large and small orbital inclination[6] ($\theta_m = 20°$ and $\theta_m = 70°$). We then vary p to study radiation emission from four different resonances, 3:1, 2:1, 3:2, and 4:3. The fractional variation in a quantity X is defined as

$$\Delta X \equiv \frac{|X_{\max}| - |X_{\min}|}{(|X_{\max}| + |X_{\min}|)/2}, \tag{4.5}$$

where $X_{\max\,/\,\min}$ is the maximum or minimum value X takes as χ_0 varies from 0 to 2π.

The peak-to-trough variation (4.5) in the fluxes is an important quantity that determines several properties of the resonances. First, the "kicks" in E, L_z, and Q that occur as a system spirals through a resonance are directly proportional to the variation (4.5) [39]. As such, these quantities give some idea of how much impact resonances will have as a system evolves through orbit, even though we have not yet developed the tools needed to compute these evolutions in detail. Second, there are two qualitatively different types of resonances that can occur in systems of this kind: a simple linear resonance in which the kicks depend sinusoidally on the phase parameter χ_0 (cf. the final equation of FH) and a nonlinear variant in which the dynamics is rather more complicated. For the nonlinear scenario, it is possible to have a "sustained resonance" in which the system becomes trapped near the resonance for an extended period of time [40,41]. Our numerical results show that $\Delta X \ll 1$ at least over all of the parameter space we have surveyed so far, which indicates that the resonances are always of the simple, linear kind. This agrees with post-Newtonian analyses [39], as well as recent work by van de Meent [42].

Some interesting trends are apparent from these tables. First, notice that in all cases the down-horizon variation is quite a bit larger than than the variation in the quantities to infinity. However, in all cases, the magnitude of the down-horizon fluxes is substantially smaller than the magnitude to infinity. The total variations are thus dominated by the fluxes to infinity, consistent with the results shown in Fig. 5.

Second, notice that the largest variations are seen in either the 2:1 or 3:2 resonances (always the 3:2 resonance for orbits with $e = 0.3$, but either 3:2 or 2:1 depending on which quantity we examine for the orbits with $e = 0.7$). The variations are consistently smallest for the 4:3 resonance. This behavior correlates with the shape that a resonant orbit traces in the (r, θ) plane. Figure 6 shows these orbital tracks for the four orbits presented in Table I. For simplicity, we only show tracks for $\chi_0 = \pi/2$.

The contrasting shapes of the 2:1 and 3:2 orbits on one hand, and of the 4:3 orbit on the other, are particularly noteworthy. The 4:3 resonant orbit (bottom right) traces a rather complicated Lissajous figure which comes "close to" many of the (r, θ) points which are accessible given (p, e, θ_m). This complicated trajectory samples much of the accessible domain in r and θ. Appealing to the constrained integral method of computing $\mathcal{Z}_{lmN}^\star$ (cf. Sec. III D), we can say that the motion effectively averages out the variations in the integrand by passing close to so many accessible points.

By contrast, the trajectory for the 2:1 and 3:2 resonances (top right and bottom left) are much simpler. These trajectories do not come as close to so many points in their allowed domain, and so do not average the variations in their integrands as effectively. The trajectory for the 3:1 (top left) resonance is similar to that for the 2:1 case, but with an additional angular oscillation at small radius. This extra oscillation enhances the averaging as the orbit moves through a particularly strong-field part of its domain. Not

[6]Note that smaller θ_m implies a more highly inclined orbit; $\theta_m = 90°$ is an equatorial orbit.

TABLE I. Variation in flux for orbits with $e = 0.7$ and $\theta_m = 20°$ about a black hole with spin $a = 0.9M$. We vary p to examine a sequence of orbital resonances from $\Omega_\theta/\Omega_r = 3$ to $\Omega_\theta/\Omega_r = 4/3$. Columns 3–5 show the fractional variation in energy flux, axial angular momentum flux, and Carter constant rate of change arising from the down-hole fields; the fractional variation is defined precisely in the text. Columns 6–8 repeat this information for these fields at infinity, and columns 9–11 give the fractional variation for the totals (infinity plus horizon). The variations are largest for the 3:2 resonance and 2:1 resonances (depending on which quantity we examine), and smallest for the 4:3 resonance.

e	θ_m	p	Ω_θ/Ω_r	$\Delta\dot{E}^H$	$\Delta\dot{L}_z^H$	$\Delta\dot{Q}^H$	$\Delta\dot{E}^\infty$	$\Delta\dot{L}_z^\infty$	$\Delta\dot{Q}^\infty$	$\Delta\dot{E}^{\rm tot}$	$\Delta\dot{L}_z^{\rm tot}$	$\Delta\dot{Q}^{\rm tot}$
0.7	20°	5.38952M	3	92.5%	0.363%	0.543%	0.087%	0.069%	0.105%	0.125%	0.027%	0.126%
0.7	20°	6.31541M	2	30.7%	2.89%	1.82%	0.634%	0.483%	0.467%	0.662%	0.270%	0.494%
0.7	20°	8.77436M	3/2	106%	21.9%	10.4%	1.17%	0.172%	0.219%	1.03%	0.489%	0.261%
0.7	20°	11.4219M	4/3	1.41%	0.117%	0.979%	0.048%	0.058%	0.003%	0.047%	0.060%	0.002%

TABLE II. Variation in flux for orbits with $e = 0.7$ and $\theta_m = 70°$ about a black hole with spin $a = 0.9M$. As when $e = 0.7$ and $\theta_m = 70°$, the variations are largest for the 3:2 resonance and 2:1 resonances (depending on which quantity we examine), and smallest for the 4:3 resonance.

e	θ_m	p	Ω_θ/Ω_r	$\Delta\dot{E}^H$	$\Delta\dot{L}_z^H$	$\Delta\dot{Q}^H$	$\Delta\dot{E}^\infty$	$\Delta\dot{L}_z^\infty$	$\Delta\dot{Q}^\infty$	$\Delta\dot{E}^{\rm tot}$	$\Delta\dot{L}_z^{\rm tot}$	$\Delta\dot{Q}^{\rm tot}$
0.7	70°	3.27580M	3	1.14%	1.89%	2.60%	0.010%	0.067%	0.421%	0.026%	0.009%	0.035%
0.7	70°	3.78947M	2	1.60%	2.68%	6.01%	0.204%	0.153%	0.109%	0.167%	0.067%	0.357%
0.7	70°	5.48622M	3/2	6.66%	5.77%	26.3%	0.222%	0.034%	0.216%	0.127%	0.078%	0.210%
0.7	70°	7.53814M	4/3	0.042%	0.008%	4.04%	0.001%	0.002%	0.023%	0.001%	0.002%	0.023%

TABLE III. Variation in flux for orbits with $e = 0.3$ and $\theta_m = 20°$ about a black hole with spin $a = 0.9M$. In this case, the 3:2 resonance shows larger variations than all other cases; the 2:1 resonance is surprisingly weak, given its strength in other examples we have seen. As usual, however, the 4:3 resonance shows the least amount of variation among all the resonances that we consider.

e	θ_m	p	Ω_θ/Ω_r	$\Delta\dot{E}^H$	$\Delta\dot{L}_z^H$	$\Delta\dot{Q}^H$	$\Delta\dot{E}^\infty$	$\Delta\dot{L}_z^\infty$	$\Delta\dot{Q}^\infty$	$\Delta\dot{E}^{\rm tot}$	$\Delta\dot{L}_z^{\rm tot}$	$\Delta\dot{Q}^{\rm tot}$
0.3	20°	5.04884M	3	4.43%	0.659%	1.15%	0.027%	0.068%	0.054%	0.008%	0.024%	0.033%
0.3	20°	6.12789M	2	4.24%	1.42%	1.94%	0.012%	0.025%	0.013%	0.004%	0.080%	0.002%
0.3	20°	8.65334M	3/2	3.34%	2.62%	8.82%	0.308%	0.158%	0.114%	0.303%	0.123%	0.123%
0.3	20°	11.3158M	4/3	0.104%	0.165%	1.09%	0.003%	0.005%	0.002%	0.003%	0.004%	0.002%

TABLE IV. Variation in flux for orbits with $e = 0.3$ and $\theta_m = 70°$ about a black hole with spin $a = 0.9M$. The case is qualitatively similar to most of the others, with the 3:2 and 2:1 showing the largest degree of variation (depending on the quantity being examined), and the 4:3 case showing the least.

e	θ_m	p	Ω_θ/Ω_r	$\Delta\dot{E}^H$	$\Delta\dot{L}_z^H$	$\Delta\dot{Q}^H$	$\Delta\dot{E}^\infty$	$\Delta\dot{L}_z^\infty$	$\Delta\dot{Q}^\infty$	$\Delta\dot{E}^{\rm tot}$	$\Delta\dot{L}_z^{\rm tot}$	$\Delta\dot{Q}^{\rm tot}$
0.3	70°	2.91117M	3	1.13%	1.17%	0.544%	0.023%	0.026%	0.367%	0.059%	0.070%	0.310%
0.3	70°	3.55601M	2	1.10%	1.28%	3.67%	0.103%	0.142%	0.039%	0.131%	0.179%	0.046%
0.3	70°	5.34138M	3/2	0.481%	0.336%	4.86%	0.106%	0.063%	0.227%	0.102%	0.067%	0.208%
0.3	70°	7.41979M	4/3	0.007%	0.021%	0.229%	0.001%	0.001%	0.006%	0.001%	0.001%	0.006%

too surprisingly, the flux variation in this case is generally intermediate to the others.

Beyond the fact that orbits with simple shapes in the (r, θ) plane tend to show stronger resonances than orbits with more complicated shapes, we do not as yet see strong evidence of any trend which would allow us to predict which resonances will tend to be "strong" (i.e., exhibit large variation in orbital parameter evolution) and which will tend to be "weak." Consider for example the rate of change of orbital energy, $\Delta\dot{E}^{\rm tot}$. As we go from high inclination to shallow and from high eccentricity to low, we see that $\Delta\dot{E}^{\rm tot}$ goes from large to small: It takes the value 1.03% for high eccentricity, high inclination (Table I); 0.167% and 0.303% for the mixed cases (Tables II and III); and the value

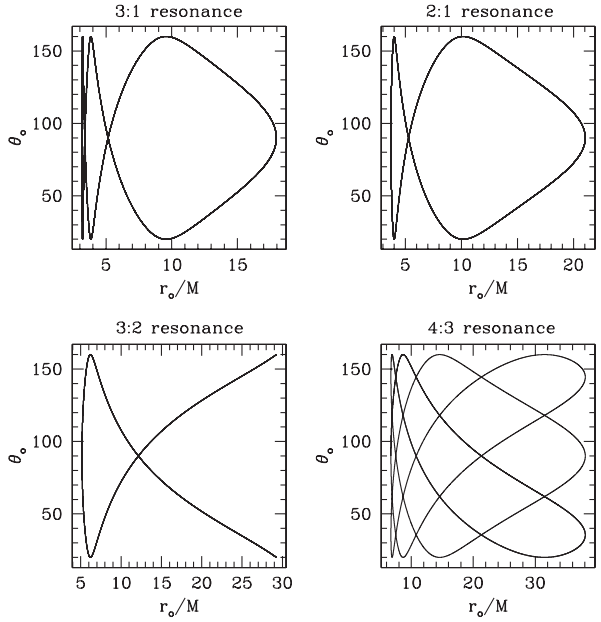

FIG. 6. Trajectories in the (r, θ) plane for the orbits discussed in Table I. We put $\chi_0 = \pi/2$ for these plots. The 4:3 resonance shows the smallest flux variation of those considered here, and has the most complicated trajectory. This orbit comes "close to" enough points in the (r, θ) plane that it averages over much of its accessible domain. By contrast, the 3:2 and 2:1 orbits have simple trajectories and do not effectively average over their domain. Fluxes from these orbits tend to show the largest variation with χ_0. The 3:1 orbit is similar to the 2:1 orbit, but with an additional angular oscillation at small radius which enhances orbital averaging. This orbit generally shows intermediate flux variation compared with the other cases.

0.131% for the case of small eccentricity, shallow inclination (Table IV). This appears to suggest, at least roughly, that the strength of the resonance is correlated with the degree of radial and angular motion.

However, no such pattern is seen when we examine $\Delta\dot{L}_z^{\rm tot}$ and $\Delta\dot{Q}^{\rm tot}$. For L_z, the high eccentricity, high inclination case again produces the largest variation (0.489%, in the 3:2 resonance of Table I). However, the *low* eccentricity, *low* inclination case produces the second largest variation (0.123%, in the 3:2 resonance of Table IV). These values of e and θ_m likewise produce the largest and second-largest variations in the Carter constant (albeit in different resonances).

We do not yet have a compelling way to explain these trends (or lack of trends) in the resonances' strength, so we leave this mystery to future work.

V. CONCLUDING DISCUSSION AND FUTURE WORK

In this analysis, using a Teukolsky-equation-based formalism good for exploring radiation produced by strong-field orbits, we have confirmed the picture that on resonance the gravitational-wave driven evolution of a binary can depend strongly on the relative phase of radial and angular motions. A binary in which this relative phase has the value $\pi/2$ as the system enters resonance may evolve quite differently from an otherwise identical system in which this phase is $3\pi/2$ entering resonance. A typical extreme mass-ratio binary can be expected to pass through several orbital resonances en route to its final coalescence. That their evolution through each resonance depends strongly on an "accidental" phase parameter has the potential to complicate schemes for measuring gravitational waves from these binaries.

We find that the degree of variation depends strongly upon the topology of the orbital trajectory in the (r, θ) plane.[7] Of the cases we have studied in detail, the orbital plane trajectory of resonances like $\Omega_\theta/\Omega_r = 3/2$ have a simple topology. This trajectory does not cross itself very often, and does not come close to many points in the plane. Such resonances do not effectively average out the behavior of the source to the wave equation. As such, if the source varies significantly over an orbit, there can be a strong residue of this variation in the associated radiation. By contrast, the trajectory of resonances like $\Omega_\theta/\Omega_r = 4/3$ has a more complicated topology, crossing itself many times, and more completely "covering" the plane. In these cases, the orbit comes "close to" many of the allowed points in the (r, θ) plane, which quite effectively averages out the source's behavior.

Although instructive and a nice validation of our ability to examine resonances, these results are not enough to truly assess the importance that resonances have in a strong field analysis. We must be able to analyze a system as it evolves through a resonance, and thereby integrate the full "kicks" in the integrals of motion E, L_z, and Q imparted to the system as it passes through resonance. A first step in this direction has been taken by van de Meent [42], who examines the likelihood that resonances can "trap" an orbit, leading to long-lived resonant waves. Part of van de Meent's analysis is a description of the system's evolution as motion through a one-dimensional effective potential. This approach is likely to be useful for more general analysis of resonant evolution.

For our planned work, we have begun expanding our Teukolsky code to compute, in the frequency domain, the instantaneous components of the dissipative or radiative piece of the self-force. Our formulation is based in part on the discussion of Refs. [14,15,21], but generalized to compute the full dissipative self-force rather than its torus

[7]Strictly speaking, it is a trajectory's geometry that matters, particularly how close the orbit comes to all accessible points in the (r, θ) plane. However, its geometry is strongly correlated to its topology, which is an invariant property of a resonant orbit's frequencies [17]. As such, the topology is a valuable way to characterize this aspect of its resonant behavior.

average.[8] This will allow us to study how a real inspiral is affected as we evolve through each resonance using results that are good deep in the strong field. The results shown in this paper are a first step toward this, demonstrating that our strong-field toolkit can be used to study resonant effects.

ACKNOWLEDGMENTS

The code used here was developed from that used for Ref. [23]; we thank Steve Drasco for his contributions to that work and the development of this code. We thank Tanja Hinderer, Amos Ori, Nicolás Yunes, and Janna Levin for useful discussions in the course of this research, and Leor Barack and Maarten van de Meent for pointing out a minor error regarding the magnitude of orbital frequencies for generic orbits. We particularly thank Gabriel Perez-Giz, whose discussion of how the on-resonant fluxes should average away was helpful in tracking down a bug in our analysis, and Rebecca Grossman for detailed and helpful discussions regarding Ref. [18]. We also thank the referees, whose feedback enabled us to significantly improve presentation of our results. Our work was supported at MIT by NSF Grant No. PHY-1068720 and by NASA Grant No. NNX08AL42G, and at Cornell by NSF Grant No. PHY-1068541. S. A. H. gratefully acknowledges fellowship support by the John Simon Guggenheim Memorial Foundation, and sabbatical support from the Canadian Institute for Theoretical Astrophysics and the Perimeter Institute for Theoretical Physics. U. R. gratefully acknowledges fellowship support from the Royal Thai Government.

APPENDIX A: PROOF: EQUIVALENCE OF METHODS FOR COMPUTING ON-RESONANT AMPLITUDES

In this appendix, we prove that Eq. (3.45), the 1-D integral for the on-resonance 3-index amplitude $\mathcal{Z}^{\star}_{lmN}(\chi_0)$, is equivalent to Eq. (3.34), the on-resonance amplitude expressed as a sum of 4-index amplitudes $Z^{\star}_{lmkn}(\chi_0)$, each of which is computed using the 2-D integral (3.14). Similar discussion, demonstrating the equivalence of these forms of the amplitudes, can be found in Appendix B of Ref. [18].

We begin with Eq. (3.6), which we repeat here:

$$Z^{\star}_{lm\omega}(\chi_0) = C^{\star}\int_{-\infty}^{\infty} d\lambda e^{i(\omega\Gamma - m\Upsilon_\phi)\lambda} J^{\star}_{lm\omega}[r_o(\lambda),\theta_o(\lambda,\chi_0)]. \tag{A1}$$

Recall that the "o" subscript on r and θ means that those are quantities along the orbit and, as such, vary at harmonics of the frequencies Υ_r and Υ_θ. We can thus expand $J^{\star}_{lm\omega}$ in a Fourier series:

$$J^{\star}_{lm\omega} = \sum_{kn} J^{\star}_{\omega lmkn}(\chi_0) e^{-i(k\Upsilon_\theta + n\Upsilon_r)\lambda}, \tag{A2}$$

$$= \sum_{N} \mathcal{J}^{\star}_{\omega lmN}(\chi_0) e^{-iN\Upsilon\lambda}. \tag{A3}$$

Equation (A2) holds for arbitrary orbits. Equation (A3) only holds on resonance, when $\Upsilon_\theta = \beta_\theta\Upsilon$, $\Upsilon_r = \beta_r\Upsilon$.

Because Eq. (A2) remains valid for resonant orbits, in the resonant case

$$\sum_{N} \mathcal{J}^{\star}_{\omega lmN}(\chi_0) e^{-iN\Upsilon\lambda} \doteq \sum_{kn} J^{\star}_{\omega lmkn}(\chi_0) e^{-i(k\Upsilon_\theta + n\Upsilon_r)\lambda}. \tag{A4}$$

(The notation "$\doteq$" means that this equation is true only on resonance.) Multiply both sides by $e^{iN'\Upsilon\lambda}$ and integrate from 0 to $2\pi/\Upsilon$. On the left-hand side, we have

$$\int_0^{2\pi/\Upsilon} \sum_N \mathcal{J}^{\star}_{\omega lmN}(\chi_0) e^{i(N'-N)\Upsilon\lambda} d\lambda = \frac{2\pi}{\Upsilon}\sum_N \mathcal{J}^{\star}_{\omega lmN}(\chi_0)\delta_{NN'} = \frac{2\pi}{\Upsilon}\mathcal{J}^{\star}_{\omega lmN'}(\chi_0). \tag{A5}$$

To do this operation on the right-hand side, first note that by the resonance condition we must have

$$k\Upsilon_\theta + n\Upsilon_r = (k\beta_\theta + n\beta_r)\Upsilon. \tag{A6}$$

Using this, the integral for the right-hand side becomes

$$\int_0^{2\pi/\Upsilon} \sum_{kn} J^{\star}_{\omega lmkn}(\chi_0) e^{i[N' - (k\beta_\theta + n\beta_r)]\Upsilon\lambda} d\lambda = \frac{2\pi}{\Upsilon}\sum_{kn} J^{\star}_{\omega lmkn}(\chi_0)\delta_{(k\beta_\theta + n\beta_r),N'} = \frac{2\pi}{\Upsilon}\sum_{(k,n)_{N'}} J^{\star}_{\omega lmkn}(\chi_0). \tag{A7}$$

The notation $(k,n)_{N'}$ means that the sum is over all pairs (k,n) which satisfy $k\beta_\theta + n\beta_r = N'$.

Next, use Eqs. (3.13), (3.15), and (3.44), invoke Eq. (3.34), drop the primes on the index N, and equate (A5) and (A7). The result is

$$\mathcal{Z}^{\star}_{lmN}(\chi_0) \doteq \sum_{(k,n)_N} e^{i\xi_{mkn}(\chi_0)} \check{Z}^{\star}_{lmkn}, \tag{A8}$$

which proves that the 1-D integral and the sum of 2-D integrals are equivalent for resonant orbits.

APPENDIX B: EVOLUTION OF THE CARTER CONSTANT

The third conserved quantity associated with orbits of Kerr black holes is the Carter constant, Q. Rearranging Eq. (2.2), we write

[8] One might be concerned about gauge ambiguities associated with the gravitational self-force. As shown by Mino [11], these ambiguities disappear when one averages the self-force's effects over an infinite time. In a two-time scale expansion [12], such ambiguities remain, but are suppressed by the ratio of the time scales.

$$Q = \cot^2\theta L_z^2 + \cos^2\theta(1-E^2) + \left(\frac{d\theta}{d\lambda}\right)^2. \tag{B1}$$

Reference [25] (S06) first demonstrated how to compute the long-time-averaged evolution of Q, at least for nonresonant orbits. In this appendix, we revisit their calculation in some detail in order to see clearly how it will have to be modified for resonant orbits (modifying some details to be in accord with our notation). We then examine how the calculation changes when we are on an orbital resonance.

1. A comment regarding averaging

In this and the following appendix, we average several quantities, defining

$$\langle f\rangle = \lim_{L\to\infty}\frac{1}{2L}\int_{-L}^{L} d\lambda f(\lambda) \tag{B2}$$

for various functions $f = f[r(\lambda),\theta(\lambda)]$. For nonresonant orbits (i.e, those in which Ω_θ/Ω_r is an irrational number), the average (B2) is equivalent to the torus average:

$$\langle f\rangle_{\text{non-res}} = \frac{\Upsilon_\theta\Upsilon_r}{(2\pi)^2}\int_0^{2\pi/\Upsilon_\theta}\int_0^{2\pi/\Upsilon_r} f[r(\lambda^r),\theta(\lambda^\theta)]d\lambda^r d\lambda^\theta. \tag{B3}$$

If the orbit's frequencies are commensurate (i.e., if it is a resonant orbit), (B2) is equivalent to the average over the 1-D trajectory that the orbit traces on the $(\lambda^r, \lambda^\theta)$ torus:

$$\langle f\rangle_{\text{res}} = \frac{\Upsilon}{2\pi}\int_0^{2\pi/\Upsilon} f[r(\lambda),\theta(\lambda,\chi_0)]d\lambda. \tag{B4}$$

Notice that in the resonant case, the average depends on the offset phase χ_0. As such, if we imagine evolving from a nonresonant to a resonant orbit, $\langle f\rangle$ will not change smoothly. Instead, it will jump discontinuously as we move from the orbit in which $\langle f\rangle$ does not depend on χ_0 to the one where it does so depend, and, the amount of jump will depend on the specific value of χ_0 we have chosen.

This discontinuous jumping behavior is an artifact of the infinite time average, a limit which is of course irrelevant for a real astrophysical inspiral. A real system will spend some finite time near any given orbit; if one wants to study averaged quantities, these quantities should be averaged over something like that finite time.

As such, it should be understood that the infinite time averages that we discuss in this paper are not intended to serve as tools to be used for evolving extreme mass-ratio binaries through resonances. For that purpose, we instead advocate direct integration of the equations of motion including self-force—without any averaging. The infinite time averaged rates of change we compute here are intended solely as diagnostics of how a system's evolution is changed by resonant physics, and how that change depends on the phase χ_0.

2. Setup

We begin with the first line of Eq. (3.18) of S06. It relates the averaged rate of change of the Carter constant, per unit Mino time, to the Kerr metric's Killing tensor $K^{\alpha\beta}$ and to a radiative field Ψ_{rad} which is constructed from the perturbation to the Kerr spacetime metric:

$$\left\langle\frac{dK}{d\lambda}\right\rangle \equiv \lim_{L\to\infty}\frac{1}{2L}\int_{-L}^{L} d\lambda\frac{dK}{d\lambda} = \lim_{L\to\infty}\frac{1}{2L}\int_{-L}^{L} d\lambda\left[2\Sigma K^{\alpha\beta}\tilde{u}_\alpha\partial_\beta\left(\frac{\Psi_{\text{rad}}}{\Sigma}\right)\right]\Bigg|_{x\to z(\lambda)}. \tag{B5}$$

We refer the reader to S06 for a detailed derivation of Eq. (B5), and defer discussion of the radiative field $\Psi_{\text{rad}}(x)$ to Secs. B 4 and B 5. The coordinate x represents a general spacetime field point; $x\to z(\lambda)$ means to take this general point to the orbit's worldline $z(\lambda)$.

The other quantities appearing in Eq. (B5) are as follows: First, K is a variant of the Carter constant, given by

$$K = Q + (L_z - aE)^2. \tag{B6}$$

It is related to the Kerr metric's Killing tensor by

$$K = K^{\alpha\beta}u_\alpha u_\beta, \tag{B7}$$

where

$$K^{\alpha\beta} = 2\Sigma m^{(\alpha}\bar{m}^{\beta)} - a^2\cos^2\theta g^{\alpha\beta}. \tag{B8}$$

The tensor $g^{\alpha\beta}$ is the Kerr metric, and m^α are components of the Newman-Penrose tetrad leg,

$$m^t = \frac{ia\sin\theta}{\sqrt{2}(r+ia\cos\theta)}, \qquad m^r = 0,$$
$$m^\theta = \frac{1}{\sqrt{2}(r+ia\cos\theta)}, \qquad m^\phi = \frac{i\csc\theta}{\sqrt{2}(r+ia\cos\theta)}. \tag{B9}$$

The overbar denotes a complex conjugate. The quantity $\tilde{u}_\alpha$ is the 4-velocity promoted to a spacetime field:

$$(\tilde{u}_t,\tilde{u}_r,\tilde{u}_\theta,\tilde{u}_\phi) = (-E,\pm\sqrt{R(r)}/\Delta,\pm\sqrt{\Theta(\theta)},L_z), \tag{B10}$$

where $R(r)$ is defined in Eq. (2.1), and $\Theta(\theta)$ in Eq. (2.2). Notice that our $\tilde{u}_\theta$ differs from that used in S06. This is due to a difference in the definition of the potential Θ (it describes motion in θ here, but motion in $\cos\theta$ in S06). The

field $\tilde{u}_\alpha$ reduces exactly to the 4-velocity u_α when we take the limit of the field point x to the worldline $z(\lambda)$.

3. General simplification

We now take the first steps in simplifying Eq. (B5). These steps are the same for both resonant and nonresonant cases; we specialize to those cases in Secs. B 4 and B 5.

We begin by focusing on the integrand of Eq. (B5):

$$\left[2\Sigma K^{\alpha\beta}\tilde{u}_\alpha\partial_\beta\left(\frac{\Psi_{\rm rad}}{\Sigma}\right)\right]\Big|_{x\to z(\lambda)} = \left[4\Sigma^2 m^{(\alpha}\bar{m}^{\beta)}\tilde{u}_\alpha\partial_\beta\left(\frac{\Psi^{\rm rad}}{\Sigma}\right) - 2\Sigma a^2\cos^2\theta\tilde{u}^\alpha\partial_\alpha\left(\frac{\Psi^{\rm rad}}{\Sigma}\right)\right]\Big|_{x\to z(\lambda)}. \tag{B11}$$

Use the fact that $\tilde{u}^\alpha = u^\alpha$ in the limit $x \to z(\lambda)$, and that $\Sigma u^\alpha = dx^\alpha/d\lambda$. Expanding $m^{(\alpha}\bar{m}^{\beta)}$, we find

$$2\Sigma K^{\alpha\beta}\tilde{u}_\alpha\partial_\beta\left(\frac{\Psi_{\rm rad}}{\Sigma}\right) = 2\Sigma\left[(L_z - a\sin^2\theta E)(\csc^2\theta\partial_\phi + a\partial_t) + \frac{d\theta}{d\lambda}\partial_\theta\right]\left(\frac{\Psi^{\rm rad}}{\Sigma}\right) - 2a^2\cos^2\theta\frac{d}{d\lambda}\left(\frac{\Psi^{\rm rad}}{\Sigma}\right). \tag{B12}$$

[For brevity, we omit $x \to z(\lambda)$ in Eqs. (B12) and (B13), though it should be understood that this limit is taken.] The right-hand side of Eq. (B12) can be simplified significantly by combining the term in $d\theta/d\lambda$ with the final term:

$$2\Sigma\frac{d\theta}{d\lambda}\partial_\theta\left(\frac{\Psi^{\rm rad}}{\Sigma}\right) - 2a^2\cos^2\theta\frac{d}{d\lambda}\left(\frac{\Psi^{\rm rad}}{\Sigma}\right) = 2\frac{d\theta}{d\lambda}\partial_\theta\Psi_{\rm rad} - 2\frac{\Psi^{\rm rad}}{\Sigma}\frac{d\theta}{d\lambda}\partial_\theta\Sigma - 2a^2\frac{d}{d\lambda}\left(\cos^2\theta\frac{\Psi^{\rm rad}}{\Sigma}\right) + 2a^2\frac{\Psi^{\rm rad}}{\Sigma}\frac{d}{d\lambda}(\cos^2\theta). \tag{B13}$$

The third term on the right-hand side of Eq. (B13) is a total derivative in $d/d\lambda$. Thanks to the periodic nature of all the relevant terms, it will not contribute to an averaging integral of the form (B5), and may be discarded. Using

$$\partial_\theta\Sigma = a^2\partial_\theta\cos^2\theta, \qquad \frac{d}{d\lambda}\cos^2\theta = \frac{d\theta}{d\lambda}\partial_\theta\cos^2\theta, \tag{B14}$$

we see that the second and fourth terms on the right-hand side of (B13) cancel; only the term in $\partial_\theta\Psi_{\rm rad}$ remains. The integrand simplifies to

$$\left[2\Sigma K^{\alpha\beta}\tilde{u}_\alpha\partial_\beta\left(\frac{\Psi_{\rm rad}}{\Sigma}\right)\right]\Big|_{x\to z(\lambda)} = \left\{2\left[(L_z - a\sin^2\theta E)(\csc^2\theta\partial_\phi + a\partial_t) + \frac{d\theta}{d\lambda}\partial_\theta\right]\Psi_{\rm rad}\right\}\Big|_{x\to z(\lambda)}. \tag{B15}$$

The radiative field $\Psi_{\rm rad}$ can be broken into an "out" and a "down" component:

$$\Psi_{\rm rad} = \Psi^{\rm out}_{\rm rad} + \Psi^{\rm down}_{\rm rad}. \tag{B16}$$

These two fields are in turn computed from mode functions $\Phi_{lm\omega}$ (discussed in more detail momentarily) as follows:

$$\Psi^{\rm out}_{\rm rad}(x) = \int d\omega\sum_{lm}\frac{1}{4i\omega^3}\left[\Phi^{\rm out}_{lm\omega}(x)\int d\lambda'\bar{\Phi}^{\rm out}_{lm\omega}[z(\lambda')]\right] + \text{c.c.}, \tag{B17}$$

$$\Psi^{\rm down}_{\rm rad} = \int d\omega\sum_{lm}\frac{1}{4i\omega^2 p_m}\left[\Phi^{\rm down}_{lm\omega}(x)\int d\lambda'\bar{\Phi}^{\rm down}_{lm\omega}[z(\lambda')]\right] + \text{c.c.} \tag{B18}$$

In Eq. (B18), $p_m = \omega - m\Omega_H$, where $\Omega_H = a/2Mr_+$ is the angular velocity associated with the event horizon. The abbreviation "c.c." means complex conjugate. See S06 for further discussion and derivation of these forms of the fields $\Psi^{\rm out}_{\rm rad}$ and $\Psi^{\rm down}_{\rm rad}$. We will largely focus on the "out" field, which is related to radiation at $\mathcal{I}^+$. Extension to the "down" field, related to radiation on the event horizon, is straightforward.

To proceed, we use two equivalent forms for $\Phi^{\rm out}_{lm\omega}(x)$ evaluated in the limit $x \to z(\lambda)$; both are described in more detail in S06. The first is up to a constant factor the complex conjugate of the integrand in the expression (3.6) for $Z^H_{lm\omega}$:

$$\Phi^{\rm out}_{lm\omega}[z(\lambda)] = \bar{J}^H_{lm\omega}(\lambda)e^{-i\lambda(\Gamma\omega - m\Upsilon_\phi)}. \tag{B19}$$

Here Γ is the factor introduced in Sec. II B that converts the mean accumulation of Mino time to the mean accumulation of coordinate time. Equation (B19) is Eq. (3.11) of S06, translated into our notation[9]; the scalar-case version of this equation is Eq. (9.20) of Ref. [21]. Using the Fourier series expansion (3.10) of $J^H_{lm\omega}$, integrating with respect to λ, and combining with the definitions (3.13) and (3.15) gives

[9]Note that there are two errors in Eq. (3.11) of S06: the sign of the exponential is flipped, and the coefficients Z are of the usual type (3.15) rather than the required more general type (3.14) with $\omega \neq \omega_{mkn}$. See Eq. (B33) below.

$$\int d\lambda' \bar{\Phi}^{\rm out}_{lm\omega}[z(\lambda')] = \sum_{nk} Z^H_{lmkn}\delta(\omega-\omega_{mkn}), \tag{B20}$$

and so

$$\Psi^{\rm out}_{\rm rad}(x) = \int d\omega \left[\sum_{lmkn} \frac{Z^H_{lmkn}\delta(\omega-\omega_{mkn})}{4i\omega^3}\Phi^{\rm out}_{lm\omega}(x)\right] + \text{c.c.} \tag{B21}$$

A similar simplification describes $\Psi^{\rm down}_{\rm rad}(x)$. Combining this with Eqs. (B5) and (B15), we obtain

$$\left\langle \frac{dK^\infty}{d\lambda}\right\rangle = \left\langle \sum_{lmkn}\frac{Z^H_{lmkn}}{2i\omega^3_{mkn}}\left\{\left[(\csc^2\theta L_z - aE)\partial_\phi + a(L_z - aE\sin^2\theta)\partial_t + \frac{d\theta}{d\lambda}\partial_\theta\right]\Phi^{\rm out}_{lmkn}\right\} + \text{c.c.}\right\rangle, \tag{B22}$$

where $\Phi^{\rm out}_{lmkn} \equiv \Phi^{\rm out}_{lm\omega_{mkn}}$. (The superscript "$\infty$" is because we focus on the "out" field.)

We next manipulate the term in ∂_θ in Eq. (B22), by invoking the second form for $\Phi^{\rm out}_{lm\omega}(x)$, which is

$$\Phi^{\rm out}_{lmkn}(x) = f_{lmkn}(r,\theta)e^{im\phi}e^{-i\omega_{mkn}t}. \tag{B23}$$

The value of $f_{lmkn}(r,\theta)$ is not important for our purposes; see S06 [Eq. (3.20) and nearby text] for further details. We have changed notation from S06 slightly to highlight the fact that this function depends on l, m, k, and n; this is important for generalizing to resonant orbits. We now evaluate on the worldline $x \to z(\lambda)$, and use the following explicit representations of the motions in t and ϕ:

$$\begin{aligned} t(\lambda) &= \Gamma\lambda + \Delta t_r(\lambda) + \Delta t_\phi(\lambda), \\ \phi(\lambda) &= \Upsilon_\phi\lambda + \Delta\phi_r(\lambda) + \Delta\phi_\phi(\lambda), \end{aligned} \tag{B24}$$

cf. Eqs. (3.8) and (3.9) above and Sec. 3 of Ref. [21]. Here the function Δt_r is periodic with period Λ_r and Δt_θ is periodic with period Λ_θ, etc. This gives

$$\begin{aligned} \Phi^{\rm out}_{lmkn}(\lambda) = f_{lmkn}[r(\lambda),\theta(\lambda)]\exp\{&-i\lambda(k\Upsilon_\theta + n\Upsilon_r) \\ &- i\omega_{mkn}[\Delta t_r(\lambda) + \Delta t_\theta(\lambda)] \\ &+ im[\Delta\phi_r(\lambda) + \Delta\phi_\theta(\lambda)]\}. \end{aligned} \tag{B25}$$

We next define a mode function of two variables $(\lambda^r,\lambda^\theta)$ by

$$\begin{aligned} \Phi^{\rm out}_{lmkn}(\lambda^r,\lambda^\theta) = f_{lmkn}[r(\lambda^r),\theta(\lambda^\theta)]\exp\{&-ik\Upsilon_\theta\lambda^\theta - in\Upsilon_r\lambda^r \\ &- i\omega_{mkn}[\Delta t_r(\lambda^r) + \Delta t_\theta(\lambda^\theta)] \\ &+ im[\Delta\phi_r(\lambda^r) + \Delta\phi_\theta(\lambda^\theta)]\}. \end{aligned} \tag{B26}$$

This function is determined uniquely by the following three properties: First, it reduces to the expression (B25) when evaluated at $\lambda^r = \lambda^\theta = \lambda$; second, it is biperiodic, with a period of Λ^r in λ^r, and of Λ^θ in λ^θ; and third, it is a continuous function of the geodesic's parameters. The first two properties are sufficient to guarantee uniqueness for nonresonant orbits, but not for resonant orbits since the different periodicities become degenerate. Adding the third property is sufficient to restore uniqueness for all orbits, since resonant orbits form a set of measure zero in the phase space. See Refs. [21,30] for more details on the mapping between functions of λ and functions of $(\lambda^r,\lambda^\theta)$.

Next, differentiating the explicit expression (B26) with respect to λ^θ, we obtain the following identity relating the differential operator $d/d\lambda^\theta$ and the partial derivative operators ∂_θ, ∂_t, and ∂_ϕ acting on $\Phi^{\rm out}_{lmkn}$:

$$\frac{d\theta}{d\lambda}\partial_\theta = \frac{d}{d\lambda^\theta} + ik\Upsilon_\theta - \frac{d\Delta t_\theta}{d\lambda^\theta}\partial_t - \frac{d\Delta\phi_\theta}{d\lambda^\theta}\partial_\phi. \tag{B27}$$

We now use the identity (B27) to substitute for the $(d\theta/d\lambda)\partial_\theta$ term in Eq. (B22). This yields

$$\begin{aligned} \left\langle \frac{dK^\infty}{d\lambda}\right\rangle = \left\langle \sum_{lmkn}\frac{Z^H_{lmkn}}{2i\omega^3_{mkn}}\left\{\left[\left(\csc^2\theta L_z - aE - \frac{d\Delta\phi_\theta}{d\lambda^\theta}\right)\partial_\phi \right.\right.\right. \\ + \left(aL_z - a^2E\sin^2\theta - \frac{d\Delta t_\theta}{d\lambda^\theta}\right)\partial_t \\ \left.\left.\left. + ik\Upsilon_\theta + \frac{d}{d\lambda^\theta}\right]\Phi^{\rm out}_{lmkn}\right\} + \text{c.c.}\right\rangle. \end{aligned} \tag{B28}$$

Using Eqs. (3.43) and (3.58) of Ref. [21] it is not difficult to show that

$$\begin{aligned} \csc^2\theta L_z - aE - \frac{d\Delta\phi_\theta}{d\lambda^\theta} &= \langle \csc^2\theta L_z - aE\rangle \\ &= \langle\csc^2\theta\rangle L_z - aE, \end{aligned} \tag{B29}$$

$$\begin{aligned} aL_z - a^2E\sin^2\theta - \frac{d\Delta t_\theta}{d\lambda^\theta} &= \langle aL_z - a^2E\sin^2\theta\rangle \\ &= aL_z - a^2E\langle\sin^2\theta\rangle. \end{aligned} \tag{B30}$$

Combining this with Eq. (B28) and using the replacements $\partial_\phi \to im$, $\partial_t \to -i\omega_{mkn}$ gives

$$\left\langle \frac{dK^\infty}{d\lambda}\right\rangle = \left\langle \sum_{lmkn}\frac{Z^H_{lmkn}}{2i\omega^3_{mkn}}\left\{\left[i\mathcal{M}_{mkn} + ik\Upsilon_\theta + \frac{d}{d\lambda^\theta}\right]\Phi^{\rm out}_{lmkn}\right\} + \text{c.c.}\right\rangle, \tag{B31}$$

where we have defined

$$\mathcal{M}_{mkn} = m(\langle \csc^2\theta \rangle L_z - aE) - a\omega_{mkn}(L_z - aE\langle \sin^2\theta \rangle). \tag{B32}$$

Next, from Eqs. (B19), (3.10), (3.13), and (3.15) we obtain an expression for $\Phi^{\rm out}_{lmkn}(\lambda)$. Extending this to a function of λ^r, λ^θ as above gives

$$\Phi^{\rm out}_{lmkn}(\lambda^r, \lambda^\theta) = \frac{\Gamma}{2\pi} \sum_{\Delta n, \Delta k} \bar{Z}^H_{\omega_{mkn} lmk+\Delta k, n+\Delta n} e^{i\Delta k \Upsilon_\theta \lambda^\theta} e^{i\Delta n \Upsilon_r \lambda^r}. \tag{B33}$$

Combining this with Eq. (B31) yields the final result

$$\left\langle \frac{dK^\infty}{d\lambda} \right\rangle = \left\langle \frac{\Gamma}{4\pi} \sum_{lmkn} \sum_{\Delta k, \Delta n} [\mathcal{M}_{mkn} + k\Upsilon_\theta + \Delta k \Upsilon_\theta] \frac{Z^H_{lmkn}}{\omega^3_{mkn}} \bar{Z}^H_{\omega_{mkn} lmk+\Delta k, n+\Delta n} e^{i\Delta k \Upsilon_\theta \lambda^\theta} e^{i\Delta n \Upsilon_r \lambda^r} + \text{c.c.} \right\rangle. \tag{B34}$$

Here it is understood that the averaging procedure is to first evaluate at $\lambda^r = \lambda^\theta \equiv \lambda$ and then average over λ. In Sec. B 4, we evaluate this average for nonresonant orbits, and reproduce the results of S06. In Sec. B 5, we do so for a resonant orbit and find an appropriately modified variant of their formula.

4. Nonresonant result

We evaluate the expression (B34) at $\lambda^r = \lambda^\theta \equiv \lambda$ and then evaluate the average over λ defined by Eq. (B5). The term labeled by Δn, Δk is proportional to

$$\lim_{L\to\infty} \frac{1}{2L} \int_{-L}^{L} d\lambda e^{i\Delta k \Upsilon_\theta \lambda} e^{i\Delta n \Upsilon_r \lambda} = \lim_{L\to\infty} \mathrm{Si}[(\Delta k \Upsilon_\theta + \Delta n \Upsilon_r) L], \tag{B35}$$

where $\mathrm{Si}(x) = \sin(x)/x$. Since the frequencies Υ_θ and Υ_r are incommensurate for nonresonant orbits, the combination $\Delta k \Upsilon_\theta + \Delta n \Upsilon_r$ will be nonvanishing for $(\Delta k, \Delta n) \neq (0,0)$, and the right-hand side will vanish. Thus the only nonvanishing term will be the term with $\Delta n = \Delta k = 0$. Another way to think about this is that we are averaging over a curve which is ergodically filling up the torus parametrized by λ^r and λ^θ, and so the curve average can be replaced by an average over the torus,

$$\lim_{L\to\infty} \frac{1}{2L} \int_{-L}^{L} \ldots d\lambda \to \frac{\Upsilon_\theta \Upsilon_r}{(2\pi)^2} \int_0^{2\pi/\Upsilon_\theta} \int_0^{2\pi/\Upsilon_\theta} \ldots d\lambda^r d\lambda^\theta. \tag{B36}$$

Applying this torus average to the expression (B34) again forces $\Delta n = \Delta k = 0$. Now using the definition (3.15) we obtain the final result

$$\left\langle \frac{dK^\infty}{d\lambda} \right\rangle = \Gamma \sum_{lmkn} \frac{|\check{Z}^H_{lmkn}|^2}{4\pi\omega^3_{mkn}} [\mathcal{M}_{mkn} + k\Upsilon_\theta] + \text{c.c.} \tag{B37}$$

Because all the terms on the right-hand side of (B37) are real, the complex conjugate simplifies to an overall factor of 2. We take the long-time average, so

$$\left\langle \frac{dK}{d\lambda} \right\rangle = \Gamma \left\langle \frac{dK}{dt} \right\rangle. \tag{B38}$$

Further, by Eq. (B6),

$$\frac{dK}{dt} = \frac{dQ}{dt} + 2(aE - L_z)\left(a\frac{dE}{dt} - \frac{dL_z}{dt} \right). \tag{B39}$$

Combining Eqs. (3.25), (3.26), (3.31), (B32) together with Eqs. (B37), (B38), and (B39), we finally obtain

$$\begin{aligned} \left\langle \frac{dQ^\infty}{dt} \right\rangle &= \sum_{lmkn} \frac{|\check{Z}^H_{lmkn}|^2}{2\pi\omega^3_{mkn}} \times (m\langle \cot^2\theta \rangle L_z - a^2 \omega_{mkn} \langle \cos^2\theta \rangle E + k\Upsilon_\theta) \\ &\equiv 2 \sum_{lmkn} \frac{\dot{E}^\infty_{lmkn}}{\omega_{mkn}} (\mathcal{L}_{mkn} + k\Upsilon_\theta). \end{aligned} \tag{B40}$$

The quantity $\mathcal{L}_{mkn}$ is defined in Eq. (3.31). A similar calculation focusing on the "down" modes yields

$$\begin{aligned} \left\langle \frac{dQ^H}{dt} \right\rangle &= \sum_{lmkn} \frac{\alpha_{lmkn} |\check{Z}^\infty_{lmkn}|^2}{2\pi\omega^3_{mkn}} \times (m\langle \cot^2\theta \rangle L_z - a^2 \omega_{mkn} \langle \cos^2\theta \rangle E + k\Upsilon_\theta) \\ &= 2 \sum_{lmkn} \frac{\dot{E}^H_{lmkn}}{\omega_{mkn}} (\mathcal{L}_{mkn} + k\Upsilon_\theta). \end{aligned} \tag{B41}$$

The factor α_{lmkn} is introduced in Sec. III B; on the second line, we have used Eqs. (3.27) and (3.31). Equations (B40) and (B41) are the same (modulo minor changes in notation) as Eq. (3.26) of S06.

5. Resonant $\dot{Q}$

We now return to the general formula (B34) evaluated at $\lambda^r = \lambda^\theta = \lambda$ and compute the average over λ for the case of resonant orbits. Before evaluating this average we first simplify the sums over Δk and Δn by rewriting them in terms of $k' = k + \Delta k$, $n' = n + \Delta n$. We also make the replacements

$$\sum_{kn} \to \sum_{N} \sum_{(k,n)_N}, \qquad \sum_{k'n'} \to \sum_{N'} \sum_{(k',n')_{N'}}, \tag{B42}$$

where the indicated sums are taken over k, n satisfying $k\beta_\theta + n\beta_r = N$ and over k', n' satisfying $k'\beta_\theta + n'\beta_r = N'$. We note that the quantities $\mathcal{M}_{mkn}$ and ω_{mkn} depend on k and n only through N, and write these as $\mathcal{M}_{mN}$ and ω_{mN}. Finally using the definition (3.34) of the amplitudes $\mathcal{Z}^\star_{lmN}$, the expression (B34) reduces to

$$\left\langle \frac{dK^\infty}{d\lambda} \right\rangle = \left\langle \frac{\Gamma}{4\pi} \sum_{lmN} \sum_{N'} \sum_{(k',n')_{N'}} [\mathcal{M}_{mN} + k'\Upsilon_\theta] \times \frac{\mathcal{Z}^H_{lmN}}{\omega^3_{mN}} \bar{Z}^H_{\omega_{mkn} l m k' n'} e^{i\Delta k \Upsilon_\theta \lambda} e^{i\Delta n \Upsilon_r \lambda} + \text{c.c.} \right\rangle. \tag{B43}$$

Next we note that the argument of the exponential is

$$\begin{aligned} i\lambda(\Delta k \Upsilon_\theta + \Delta n \Upsilon_r) &= i\lambda \Upsilon (\Delta k \beta_\theta + \Delta n \beta_r) \\ &= i\lambda \Upsilon (N' - N). \end{aligned} \tag{B44}$$

Evaluating the average over λ enforces $N = N'$, and the result is

$$\left\langle \frac{dK^\infty}{d\lambda} \right\rangle = \frac{\Gamma}{4\pi} \sum_{lmN} \sum_{(k',n')_N} [\mathcal{M}_{mN} + k'\Upsilon_\theta] \times \frac{\mathcal{Z}^H_{lmN}}{\omega^3_{mN}} \bar{Z}^H_{\omega_{mkn} l m k' n'} + \text{c.c.} \tag{B45}$$

Now since $\omega_{mkn} = \omega_{mN} = \omega_{mN'}$, the factor of $\bar{Z}^H_{\omega_{mkn} l m k' n'}$ can be simplified to $\bar{Z}^H_{lmk'n'}$. The expression (B45) can then be simplified further by defining the new amplitude

$$\mathcal{Y}^H_{lmN}(\chi_0) = \sum_{(k,n)_N} k Z^H_{lmkn}(\chi_0) = \sum_{(k,n)_N} k e^{i\xi_{mkn}(\chi_0)} \check{Z}^H_{lmkn}. \tag{B46}$$

Compare this with Eq. (3.34): $\mathcal{Y}^H_{lmN}(\chi_0)$ is similar to $\mathcal{Z}_{lmN}(\chi_0)$, but with each Z^H_{lmkn} weighted by k. In terms of this new amplitude the result simplifies to

$$\left\langle \frac{dK^\infty}{d\lambda} \right\rangle = \sum_{lmN} \frac{\Gamma}{4\pi\omega^3_{mN}} [\mathcal{M}_{mN} |\mathcal{Z}^H_{lmN}(\chi_0)|^2 + \Upsilon_\theta \mathcal{Z}^H_{lmN}(\chi_0) \bar{\mathcal{Y}}^H_{lmN}(\chi_0)] + \text{c.c.} \tag{B47}$$

Applying Eqs. (B38) and (B39), we at last find the rate of change of Q for a resonant orbit:

$$\left\langle \frac{dQ^\infty}{dt} \right\rangle = \sum_{lmN} \frac{1}{2\pi\omega^3_{mN}} \{\mathcal{L}_{mN} |\mathcal{Z}^H_{lmN}(\chi_0)|^2 + \Upsilon_\theta \text{Re}[\mathcal{Z}^H_{lmN}(\chi_0) \bar{\mathcal{Y}}^H_{lmN}(\chi_0)]\}, \tag{B48}$$

where $\mathcal{L}_{mN}$ is the same as $\mathcal{L}_{mkn}$, but with $\omega_{mkn} \to \omega_{mN}$. Repeating this exercise for the "down" modes yields

$$\left\langle \frac{dQ^H}{dt} \right\rangle = \sum_{lmN} \frac{\alpha_{lmN}}{2\pi\omega^3_{mN}} \{\mathcal{L}_{mN} |\mathcal{Z}^\infty(\chi_0)|^2 + \Upsilon_\theta \text{Re}[\mathcal{Z}^\infty_{lmN}(\chi_0) \bar{\mathcal{Y}}^\infty_{lmN}(\chi_0)]\}. \tag{B49}$$

It is interesting to compare our final result for the on-resonance evolution of Q, Eqs. (B48) and (B49), with the equivalent results for the nonresonant case, Eqs. (B40) and (B41). The first two terms in both expressions for $\langle dQ/dt \rangle$ are essentially the same; going from the nonresonant case to the resonant case is simply a matter of promoting the 4-index nonresonant amplitude $Z^\star_{lmkn}$ to the 3-index resonant amplitude $\mathcal{Z}^\star_{lmN}$.

The final term in the two cases is quite different, however. In the nonresonant case, the final term is proportional to $k\Upsilon_\theta$. In the resonant case, the index k cannot appear in the final result, which can only depend on the indices l, m, and N. This is accounted for in the definition of the amplitude $\mathcal{Y}^\star_{lmN}$, Eq. (B46). In both the nonresonant and the resonant cases, this final term arises from the action of the operator $(d\theta/d\lambda)\partial_\theta$ on the radiative field Ψ_{rad} [see Eq. (B15)].

As Appendix A made clear, the 3-index amplitude $\mathcal{Z}^\star_{lmN}$ can be computed directly as a 1-D integral, Eq. (3.45), or can be computed as a sum of 4-index integrals, Eq. (3.34), each of which is computed from the 2-D integral (3.14). Our definition (B46) of $\mathcal{Y}^\star_{lmN}$ is clearly analogous to Eq. (3.34), writing this 3-index amplitude as a sum over 4-index amplitudes.

Might it be possible to compute the 3-index amplitude directly, in a manner analogous to Eq. (3.45)? We believe the answer is yes; we simply need to propagate the operator $(d\theta/d\lambda)\partial_\theta$ under the integral sign in Eq. (3.45). In other words, we speculate that

$$\mathcal{Y}^\star_{lmN}(\chi_0) \stackrel{?}{=} \frac{\Upsilon}{\Gamma} \int_0^{2\pi/\Upsilon} d\lambda \frac{d\theta}{d\lambda} \partial_\theta J^\star_{lm\omega}[r(\lambda), \theta(\lambda, \chi_0)] e^{iN\Upsilon\lambda}. \tag{B50}$$

We have not yet tested this.

APPENDIX C: RATE OF CHANGE OF E AND L_z BY DISSIPATIVE SELF-FORCE

With $\langle dQ/dt \rangle$ due to the dissipative self-force now understood, it is a relatively simple matter to likewise compute $\langle dE/dt \rangle$ and $\langle dL_z/dt \rangle$. Our calculation again

closely follows S06; the only important changes are updates to the notation that we use, and a careful analysis of resonances. The results we find are identical to the fluxes of energy and angular momentum carried by gravitational waves, exactly as Ref. [26] leads us to expect.

1. Setup

Our starting point is Eq. (3.7) of S06, which in our notation becomes

$$\left\langle \frac{dE}{d\lambda} \right\rangle \equiv \lim_{L\to\infty} \frac{1}{2L} \int_{-L}^{L} d\lambda \frac{dE}{d\lambda} = -\lim_{L\to\infty} \frac{1}{2L} \int_{-L}^{L} d\lambda [\partial_t \Psi_{\rm rad}] \Big|_{x\to z(\lambda)}. \quad \text{(C1)}$$

This equation is derived by averaging over long times the dissipative self-force contracted with the time Killing vector. Terms corresponding to total derivatives are discarded thanks to the periodic nature of the underlying functions. If we replace $-\partial_t$ with ∂_ϕ, we obtain $\langle dL_z/d\lambda \rangle$.

As in Appendix B, we will focus on the "out" fields; extension to "down" is straightforward. Using Eq. (B21),

$$\left\langle \frac{dE^\infty}{d\lambda} \right\rangle = -\left\langle \sum_{lmkn} \frac{Z^H_{lmkn}}{4i\omega^3_{mkn}} \partial_t \Phi^{\rm out}_{lmkn} + \text{c.c.} \right\rangle. \quad \text{(C2)}$$

The harmonic behavior of the mode functions means that $\partial_t \Phi^{\rm out}_{lmkn} = -i\omega_{mkn} \Phi^{\rm out}_{lmkn}$:

$$\left\langle \frac{dE^\infty}{d\lambda} \right\rangle = \left\langle \sum_{lmkn} \frac{Z^H_{lmkn}}{4\omega^2_{mkn}} \Phi^{\rm out}_{lmkn} + \text{c.c.} \right\rangle. \quad \text{(C3)}$$

Using Eq. (B33), this becomes

$$\left\langle \frac{dE^\infty}{d\lambda} \right\rangle = \left\langle \frac{\Gamma}{8\pi} \sum_{lmkn} \sum_{\Delta k,\Delta n} \frac{Z^H_{lmkn}}{\omega^2_{mkn}} \times \bar{Z}^H_{\omega_{mkn} lmk+\Delta k,n+\Delta n} e^{i\Delta k \Upsilon_\theta \lambda^\theta} e^{i\Delta n \Upsilon_r \lambda^r} + \text{c.c.} \right\rangle. \quad \text{(C4)}$$

Likewise, using $\partial_\phi \Phi^{\rm out}_{lmkn} = im\Phi^{\rm out}_{lmkn}$, we have

$$\left\langle \frac{dL^\infty_z}{d\lambda} \right\rangle = \left\langle \frac{\Gamma}{8\pi} \sum_{lmkn} \sum_{\Delta k,\Delta n} m \frac{Z^H_{lmkn}}{\omega^3_{mkn}} \times \bar{Z}^H_{\omega_{mkn} lmk+\Delta k,n+\Delta n} e^{i\Delta k \Upsilon_\theta \lambda^\theta} e^{i\Delta n \Upsilon_r \lambda^r} + \text{c.c.} \right\rangle. \quad \text{(C5)}$$

As in Appendix B, the averaging procedure we use is to evaluate at $\lambda^r = \lambda^\theta = \lambda$, and then to average over λ. We do this first for nonresonant and then for resonant orbits.

2. Nonresonant results

As in Appendix B 4, we use the fact that

$$\lim_{L\to\infty} \frac{1}{2L} \int_{-L}^{L} d\lambda e^{i\Delta k \Upsilon_\theta \lambda} e^{i\Delta n \Upsilon_r \lambda} = \lim_{L\to\infty} \text{Si}[(\Delta k \Upsilon_\theta + \Delta n \Upsilon_r) L], \quad \text{(C6)}$$

where $\text{Si}(x) = \sin(x)/x$. For nonresonant orbits, the incommensurability of Υ_θ and Υ_r means that the only nonvanishing term is $\Delta n = \Delta k = 0$, and we deduce that

$$\left\langle \frac{dE^\infty}{dt} \right\rangle = \sum_{lmkn} \frac{|Z^H_{lmkn}|^2}{4\pi\omega^2_{mkn}}, \quad \text{(C7)}$$

$$\left\langle \frac{dL^\infty_z}{dt} \right\rangle = \sum_{lmkn} \frac{m|Z^H_{lmkn}|^2}{4\pi\omega^3_{mkn}}. \quad \text{(C8)}$$

We have used the fact that the factor Γ converts, on a long-time average basis, derivatives in λ to derivatives in t. Repeating this calculation for the "down" modes, we find

$$\left\langle \frac{dE^H}{dt} \right\rangle = \sum_{lmkn} \alpha_{lmkn} \frac{|Z^\infty_{lmkn}|^2}{4\pi\omega^2_{mkn}}, \quad \text{(C9)}$$

$$\left\langle \frac{dL^H_z}{dt} \right\rangle = \sum_{lmkn} \alpha_{lmkn} \frac{m|Z^\infty_{lmkn}|^2}{4\pi\omega^3_{mkn}}. \quad \text{(C10)}$$

The factor α_{lmkn} is discussed in Sec. III B. Equations (C7)–(C10) are identical to Eqs. (3.25)–(3.28).

3. Resonant results

As in Appendix B 5, we first modify the sums by rewriting them in terms of $k' = k + \Delta k$, $n' = n + \Delta n$, and make the replacements

$$\sum_{kn} \to \sum_{N} \sum_{(k,n)_N}, \qquad \sum_{k'n'} \to \sum_{N'} \sum_{(k',n')_{N'}}, \quad \text{(C11)}$$

where the sums are taken over pairs satisfying $k\beta_\theta + n\beta_r = N$ and $k'\beta_\theta + n'\beta_r = N'$. We use the fact that ω_{mkn} depends on k and n only through N to replace it with ω_{mN}, and use the definition (3.34) of $\mathcal{Z}^\star_{lmN}$ to write (C4) as

$$\left\langle \frac{dE^\infty}{d\lambda} \right\rangle = \left\langle \frac{\Gamma}{8\pi} \sum_{lmN} \sum_{N'} \sum_{(k',n')_{N'}} \frac{\mathcal{Z}^H_{lmN}}{\omega^2_{mN}} \times \bar{Z}^H_{\omega_{mkn} lmk'n'} e^{i\Delta k \Upsilon_\theta \lambda} e^{i\Delta n \Upsilon_r \lambda} + \text{c.c.} \right\rangle. \quad \text{(C12)}$$

A similar expression describes $\langle dL_z^\infty/dt\rangle$. Using the same logic as follows Eq. (B43), we see that averaging over λ enforces $N = N'$, and we obtain

$$\left\langle \frac{dE^\infty}{dt} \right\rangle = \sum_{lmN} \frac{|\mathcal{Z}^H_{lmN}|^2}{4\pi\omega^2_{mN}}, \tag{C13}$$

$$\left\langle \frac{dL_z^\infty}{dt} \right\rangle = \sum_{lmN} \frac{m|\mathcal{Z}^H_{lmN}|^2}{4\pi\omega^3_{mN}}. \tag{C14}$$

The same analysis for the "down" modes yields

$$\left\langle \frac{dE^H}{dt} \right\rangle = \sum_{lmN} \alpha_{lmN} \frac{|\mathcal{Z}^\infty_{lmN}|^2}{4\pi\omega^2_{mN}}, \tag{C15}$$

$$\left\langle \frac{dL_z^H}{dt} \right\rangle = \sum_{lmN} \alpha_{lmN} \frac{m|\mathcal{Z}^\infty_{lmN}|^2}{4\pi\omega^3_{mN}}. \tag{C16}$$

These formulas reproduce the flux-derived results given in Sec. III C.

[1] F. Pretorius, Phys. Rev. Lett. **95**, 121101 (2005).
[2] M. Campenelli, C. O. Lousto, P. Marronetti, and Y. Zlochower, Phys. Rev. Lett. **96**, 111101 (2006).
[3] J. G. Baker, J. Centrella, D.-I. Choi, M Koppitz, and J. van Meter, Phys. Rev. Lett. **96**, 111102 (2006).
[4] S. A. Hughes, AIP Conf. Proc. **873**, 233 (2006).
[5] C. O. Lousto and Y. Zlochower, Phys. Rev. Lett. **106**, 041101 (2011).
[6] U. Sperhake, V. Cardoso, C. D. Ott, E. Schnetter, and H. Witek, Phys. Rev. D **84**, 084038 (2011).
[7] L. Barack, Classical Quantum Gravity **26**, 213001 (2009).
[8] A. Pound, E. Poisson, and B. G. Nickel, Phys. Rev. D **72**, 124001 (2005).
[9] A. Pound and E. Poisson, Phys. Rev. D **77**, 044012 (2008).
[10] E. E. Flanagan and T. Hinderer, Phys. Rev. Lett. **109**, 071102 (2012).
[11] Y. Mino, Phys. Rev. D **67**, 084027 (2003).
[12] T. Hinderer and E. E. Flanagan, Phys. Rev. D **78**, 064028 (2008).
[13] U. Ruangsri and S. A. Hughes, arXiv:1307.6483 [Phys. Rev. D (to be published)].
[14] Y. Mino, Prog. Theor. Phys. **113**, 733 (2005).
[15] T. Tanaka, Prog. Theor. Phys. Suppl. **163**, 120 (2006).
[16] T. A. Apostolatos, G. Lukes-Gerakopolous, and G. Contopoulos, Phys. Rev. Lett. **103**, 111101 (2009).
[17] R. Grossman, J. Levin, and G. Perez-Giz, Phys. Rev. D **85**, 023012 (2012).
[18] R. Grossman, J. Levin, and G. Perez-Giz, Phys. Rev. D **88**, 023002 (2013).
[19] J. R. Gair, N. Yunes, and C. M. Bender, J. Math. Phys. (N.Y.) **53**, 032503 (2012).
[20] E. E. Flanagan and T. Hinderer (work in progress).
[21] S. Drasco, E. E. Flanagan, and S. A. Hughes, Classical Quantum Gravity **22**, S801 (2005).
[22] S. A. Teukolsky, Astrophys. J. **185**, 635 (1973).
[23] S. Drasco and S. A. Hughes, Phys. Rev. D **73**, 024027 (2006).
[24] R. Fujita, W. Hikida, and H. Tagoshi, Prog. Theor. Phys. **121**, 843 (2009).
[25] N. Sago, T. Tanaka, W. Hikida, K. Ganz, and H. Nakano, Prog. Theor. Phys. **115**, 873 (2006).
[26] T. C. Quinn and R. M. Wald, Phys. Rev. D **60**, 064009 (1999).
[27] C. W. Misner, K. S. Thorne, and J. A. Wheeler, *Gravitation* (Freeman, San Francisco, 1973).
[28] W. Schmidt, Classical Quantum Gravity **19**, 2743 (2002).
[29] N. Warburton, L. Barack, and N. Sago, Phys. Rev. D **87**, 084012 (2013).
[30] S. Drasco and S. A. Hughes, Phys. Rev. D **69**, 044015 (2004).
[31] R. Fujita and W. Hikida, Classical Quantum Gravity **26**, 135002 (2009).
[32] S. A. Hughes, Phys. Rev. D **61**, 084004 (2000).
[33] R. A. Isaacson, Phys. Rev. **166**, 1272 (1968).
[34] S. A. Teukolsky and W. H. Press, Astrophys. J. **193**, 443 (1974).
[35] S. W. Hawking and J. B. Hartle, Commun. Math. Phys. **27**, 283 (1972).
[36] R. Fujita and H. Tagoshi, Prog. Theor. Phys. **112**, 415 (2004).
[37] R. Fujita and H. Tagoshi, Prog. Theor. Phys. **113**, 1165 (2005).
[38] W. Throwe, S. A. Hughes, and S. Drasco (work in progress). Preliminary version available as W. Throwe, MIT undergraduate thesis, 2010.
[39] E. E. Flanagan, T. Hinderer, S. A. Hughes, and U. Ruangsri (work in progress).
[40] A. Ori (private communication).
[41] D. L. Bosley and J. Kevorkian, SIAM J. Appl. Math. **51**, 439 (1991).
[42] M. van de Meent, arXiv:1311.4457 [Phys. Rev. D (to be published)].